N84-23752

REPORT NO. 84HV001
JANUARY 1984

PREPARED FOR MSFC
UNDER CONTRACT
NO. NAS8-33573

ANALYSIS AND CALCULATION OF MACROSEGREGATION IN A CASTING INGOT

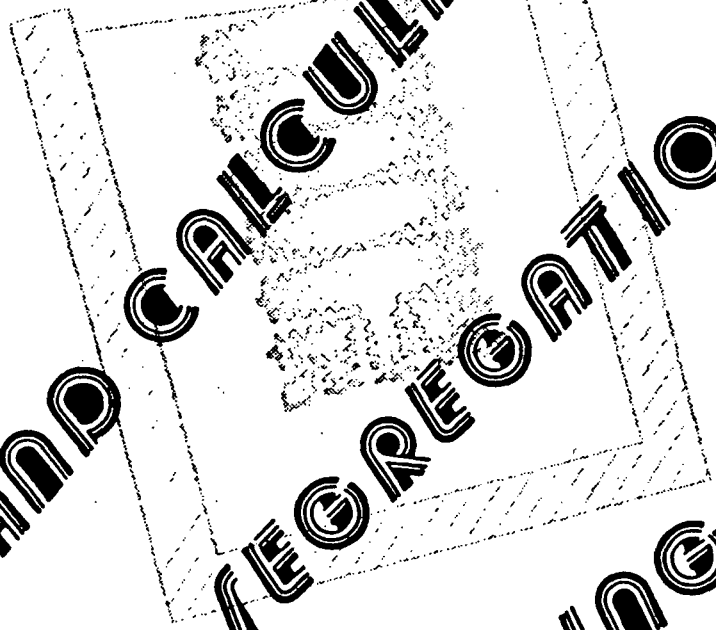

FINAL REPORT: EXHIBITS 'C' AND 'E'

PREPARED BY
GENERAL ELECTRIC COMPANY
SPACE SYSTEMS DIVISION
HUNTSVILLE OPERATIONS
HUNTSVILLE, ALABAMA

GENERAL ELECTRIC

REPORT NO: 84HV001
DATE: January 1984

MPS SOLIDIFICATION MODEL

FINAL REPORT
ANALYSIS AND CALCULATION OF MACROSEGREGATION IN A CASTING INGOT
EXHIBITS "C" AND "E"

PREPARED FOR MSFC
UNDER CONTRACT NAS8-33573

PREPARED BY:

David R Poirier
Dr. David R. Poirier
Dept. of Metallurgical Engineering
University of Arizona

Anna L. Maples
Anna L. Maples
Program Manager

APPROVED BY:

T. H. Thompson, Manager
Huntsville Operations

TABLE OF CONTENTS

TABLE OF CONTENTS (Continued)

LIST OF ILLUSTRATIONS

SECTION 1
INTRODUCTION

Over the past 15 years, researchers have established the major role in the formation of macrosegregation played by fluid flow phenomena during solidification (1-6). Calculations of macrosegregation which take into account the effects of fluid motion have achieved good agreement with experimental results for specific experimental setups (1-8). The objective of the effort reported here is to develop a computer model of solidification, including the effects of fluid flow phenomena; with application to the experimental low-g solidification program at Marshall Space Flight Center (MSFC). This effort is a continuation of the work performed under contract NAS8-33573 in which steady-state and unsteady-state models of horizontal axisymmetric bidirectional solidification were developed (9-11). These models were limited to calculation of the effects of the interdendritic fluid flow on the final macrosegregation for an input temperature field and under the assumption of no fluid flow in the bulk melt. This report describes progress toward removing these restrictions by coupling the effects of thermally induced convection in the bulk melt and of heat flow throughout the ingot to the macrosegreation calculation in the solid/liquid (S/L) region. Thus, the rate of development of the solid, a sensitive process parameter, is calculated by the model automatically; the only thermal inputs are the heat transfer coefficient at the chill and the temperature of the chill. The user does not need to measure internal temperatures for each case, an inherently difficult task for the small ingots in use at MSFC. The primary effect of the flow in the bulk melt is to change the temperature field and, thus, to alter the shape of the S/L zone and the local solidification rates. Only recently has a calculation been performed with the coupled effect of bulk liquid flow in a vertically solidified axisymmetric ingot (8). To date no published model includes the effect of maintaining the energy balance throughout the ingot coupled to a complete macrosegregation calculation.

Section 3 describes the coupling of the energy and macrosegregation equations in the S/L region, including results from one-dimensional and two-dimensional models. Due to subtleties in the nonlinear form of the macrosegregation equations required to adequately model the MSFC experiments, the anticipated

method of solution was found to be inapplicable, and in fact no existing numerical technique could be used to solve the problem. Consequently a new numerical technique was developed which is applicable to a broad class of moving boundary problems (12). This technique is implemented in a two-dimensional model of solidification of a binary alloy in a rectangular mold. The model is limited to cases which have little reverse flow in the mushy zone, i.e., cases which are far from freckle formation.

The model is implemented as an interactive program allowing on-line user selection of process parameters and alloy to be solidified, as well as the dynamic selection of graphical and tabular output. The user interface is described in Section 5; it requires minimal training and no user knowledge of programming. The code was written to provide flexibility for future development, ease of understanding to experienced programmers through readability, and efficiency of machine usage. The use of modern numerical techniques provides computational efficiency and gives fast interactive response. Documentation of the software is in Section 6.

Because of the effort expended in developing and implementing the new numerical technique, there was insufficient time to complete the calculation of flow in the bulk liquid. The preliminary analysis for this task is presented in Section 4.

SECTION 2
NOMENCLATURE

C_L	composition of the interdendritic liquid (wt. pct.)
$\bar{C}_S$	final local average composition (wt. pct.)
$C_{PL}, C_{PSL}, C_{PSE}, C_{PE}$	specific heats of the bulk liquid, interdendritic liquid, primary phase solid, and eutectic, respectively (J/gm^oC)
F, G	heat fluxes, see Eq. (3.2.1)
F_M, G_M	mass fluxes, see Eq. (3.2.4)
F_S, G_S	solute mass fluxes, see Eq. (3.2.10)
f_I, f_α, f_β	weight fraction of the intermetallic phase in the eutectic and the terminal solid solutions α and β, respectively.
g_L, g_S, g_E	volume fraction liquid, primary phase solid, and eutectic, respectively
$\vec{g}$	gravity vector (cm/s^2)
ΔH_{fi}	heat of solidification for component i (cal/mol)
H_L, H_S, H_E	specific enthalpy of the liquid, primary phase solid, and eutectic, respectively (J/gm)
H^o_{iS}, H^o_{iL}	molar enthalpies of pure component i as solid and liquid, respectively (cal/mol)
H_I	enthalpy of the intermetallic phase (cal/g)
ΔH_{298}	heat of formation at 298K (cal/mol)

J	Jacobian determinant of the coordinate transformation, see Eq. (3.2.1)
k	equilibrium partition ratio
k_T	thermal conductivity ($J/cm \cdot s \cdot {}^oC$)
K	permeability (cm^2)
M	number of equations to solve, see Eq. (3.2.31)
M_i	atomic weight of component i (gm/mol)
N_L, N_M, N_S	horizontal computational grid size in the liquid, mushy, and solid regions, respectively
N_Y	vertical computational grid size
$\vec{n}_{\Sigma E}, \vec{n}_{\Sigma L}$	unit normals to the eutectic and liquidus interfaces, respectively
p	pressure ($dynes/cm^2$)
P_0	ambient pressure, $p(X,Y)$, ($dynes/cm^2$)
q	conductive heat flux, ($J/cm^2 \cdot s$)
t	time since the beginning of solidification (s)
T, T_E, T_{L0}	temperature, eutectic temperature, temperature at the liquidus isotherm, respectively (^oC or ^oK)
$U_{\Sigma E}$	speed of the eutectic isotherm normal to itself (cm/s)
$\vec{v} = (v_X, v_Y)$	velocity of the liquid (cm/s)

x	perpendicular distance from the chill (cm)
X	dimension of the casting in the x-direction, see Fig. 3.1 (cm)
X_i	mole fraction of component i
y	distance from the "bottom" of the mold, see Fig. 3.1 (cm)
Y	dimension of the casting in the y-direction (cm)
α	thermal diffusivity (cm^2/s)
α_S, α_L	constant for the solid- and liquid-phases which is related to the heat of mixing (cal/mol)
β	volume expansion coefficient ($^oC^{-1}$)
η	transformed y-coordinate
μ	viscosity ($gm/cm \cdot s$)
ν	kinematic viscosity (cm^2/s)
ξ	transformed x-coordinate in Section 3, vorticity (S^{-1}) in Section 4
ψ	stream function (cm^2/s)
$\rho_L, \rho_S, \rho_{LE}, \rho_{SE}$	density of the liquid, primary phase solid, liquid eutectic and solid eutectic, respectively (gm/cm^3)
τ	transformed time (s)
$\vec{\Phi}$	heat flux vector which includes a conductive flux and a convective flux as defined by Eq. (3.1.9), ($J/cm^2 \cdot s$)

SECTION 3

COUPLED ENERGY CALCULATION - FORMULATION AND ANALYSIS

The central effort in the work performed under Exhibit "C" is the development of a model with the macrosegregation calculation coupled to the energy calculation. All previous macrosegregation models rely on input descriptions of the thermal field, an undesirable situation both because the measurement of the temperature field in a small ingot is an inherently difficult task and because the model predictions of macrosegregation are sensitive to temporal and spatial variations in the temperature field.

The goal of a coupled energy calculation proved to be much more difficult to accomplish than expected, primarily due to the lack of an existing numerical technique capable of handling the nonlinear complexities of the macrosegregation problem. However, the significant progress made toward this goal was achieved by developing a new numerical technique for solving problems of this type (12). The model with a coupled energy-macrosegregation calculation obtained by using the new numerical technique is reported in this section.

3.1 Physical Description

3.1.1 Problem Definition

Consider the solidification of a binary alloy in an insulated rectangular mold with a chill at one end (Fig. 3.1). In the experiments modeled here, solidification occurs over a range of temperatures so that three regions develop. The region ahead of the liquidus isotherm is entirely liquid. Between the liquidus and eutectic isotherms is a region called the mushy zone or the S/L zone which comprises the solid dendrites and solute-enriched liquid. At the eutectic isotherm a finite amount of liquid solidifies isothermally as the eutectic, and the region behind the eutectic isotherm is entirely solid.

Flow of the interdendritic liquid in the mushy zone is due to the shrinkage or expansion which accompanies solidification and to gravity acting on the density gradient within the interdendritic liquid. It is this flow of solute-rich liquid which results in the macrosegregation in the solidified casting

or ingot. The relationship between interdendritic fluid flow and macrosegregation was first described by Flemings et al. (3-5) for flow due to solidification contraction only, and later for flow driven by gravity as well as solidification contraction by Mehrabian et al. (1,6) and Kou et al. (2).

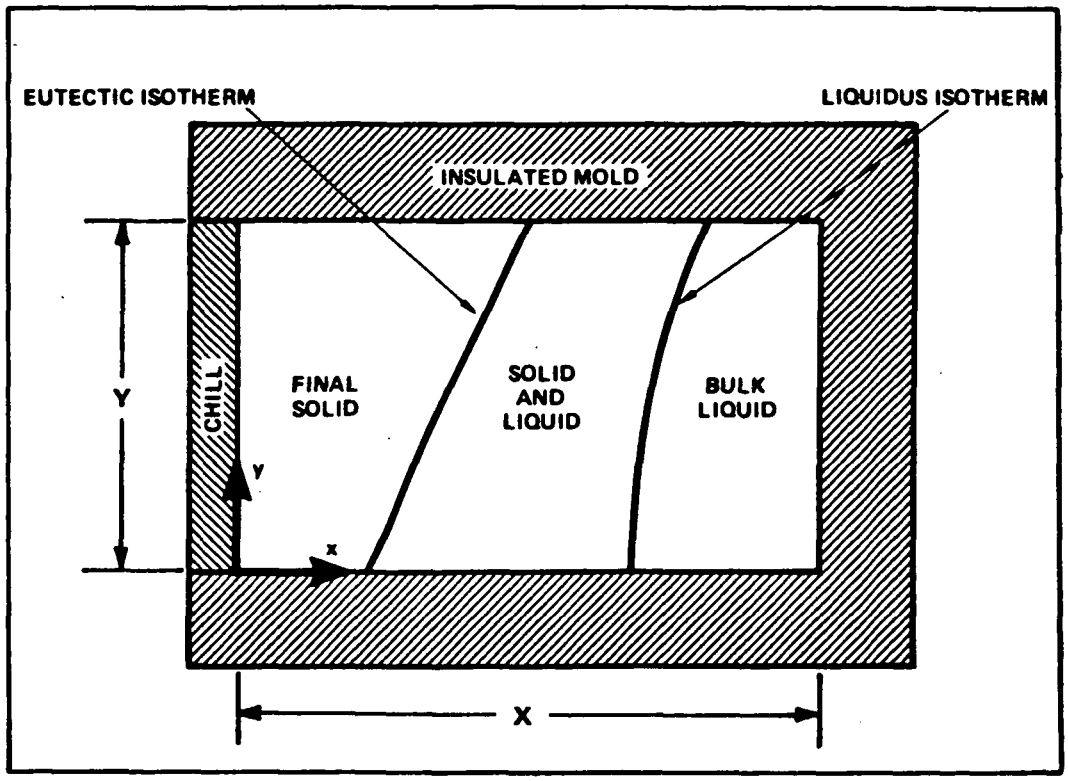

Figure 3-1. Alloy Solidification in an Axisymmetric Rectangular Mold

The solidification model described below is used to calculate the macrosegregation within the solidified casting by solving the equations for the flow of interdendritic liquid in the S/L zone coupled to the energy equation describing heat flow throughout the casting. With the exception of the addition of the energy equation the mathematical model of the flow in the S/L zone is based on the same assumptions and analysis as used in the models which were reported previously (9-11). In the S/L region of the alloy solidifying in the mold shown in Fig. 3.1, the flow of the interdendritic liquid is two-dimensional because there is no body force normal to the x-y plane. It is assumed that there is no movement of the solid; the flow of the interdendritic liquid is modeled as flow through a porous medium where the volume fraction available for flow is the local volume fraction of liquid. As

before, density is a specified function of temperature which also accounts for the variation in the composition of the interdendritic liquid.

Unlike previous models, the isotherms are not necessarily vertical. The vertical temperature gradient is caused primarily by convection of the interdendritic liquid and secondarily by the vertical variation in the thermal conductivity of the metal due to macrosegregation.

The phase diagram for the binary alloy and the thermal properties of the alloy as it solidifies along with the heat transfer coefficient at the chill are the input for the model. The temperature, pressure, velocity field, and macrosegregation are calculated by the model.

3.1.2 The Enthalpy of the Alloy and the Energy Equation

The external boundaries of the temperature field that is modeled are at the edges of the casting; heat flow in the mold is not modeled. There are two internal moving boundaries, the liquidus and eutectic isotherms, which are the locations of discontinuities in the thermal behavior of the material. Consequently there is a different energy equation for each of the three regions defined by these isotherms, and a separate relationship must be provided to describe the heat transfer across each of these moving boundaries. The location and rate of movement of the moving boundaries is not known a priori; consequently they must be calculated concurrently with the solution of the energy equations.

The energy equation for each region can be written as

$$\frac{\partial \overline{\rho H}}{\partial t} = -\nabla \cdot \vec{\Phi} \ , \qquad (3.1.1)$$

where the functional form of $\overline{\rho H}$, the enthalpy per unit volume, and $\vec{\Phi}$, the heat flux, depend on the region. Here the heat flux includes a term for the conductive flux and a term for convective flux.

In each region the enthalpy is an average of the enthalpies of the phases present weighted by volume fraction of each phase. Thus, in the liquid region

$$\overline{\rho H} = \rho_L H_L \ , \qquad (3.1.2)$$

with $$H_L = H_L^* + C_{PL}(T-T_E) \text{ for } T \geq T_E \; ; \qquad (3.1.3)$$

in the S/L zone

$$\overline{\rho H} = g_L \rho_L H_L + g_S \rho_S H_S \; , \qquad (3.1.4)$$

with H_L defined by Eq. (3.1.3) and

$$H_S = C_{PSL}\,(T-T_E); \text{ and} \qquad (3.1.5)$$

in the solid region

$$\overline{\rho H} = g_E \rho_{SE} H_E + (1-g_E)\rho_S H_S \qquad (3.1.6)$$

with $$H_S = C_{PSE}(T-T_E) \qquad (3.1.7)$$

and $$H_E = H_E^* + C_{PE}(T-T_E) \; . \qquad (3.1.8)$$

The reference enthalpies, H_L^* and H_E^* as well as the specific heats C_{PL}, C_{PSL}, C_{PSE} and C_{PE} are constants which must be specified for each alloy. Values for Al-4.5% Cu and Sn-15% Pb are given in Appendix A. The remaining variables are defined in Section 2. The relationship between temperature and enthalpy as defined by Eqs. (3.1.2)-(3.1.8) is illustrated in Fig. 3.2.

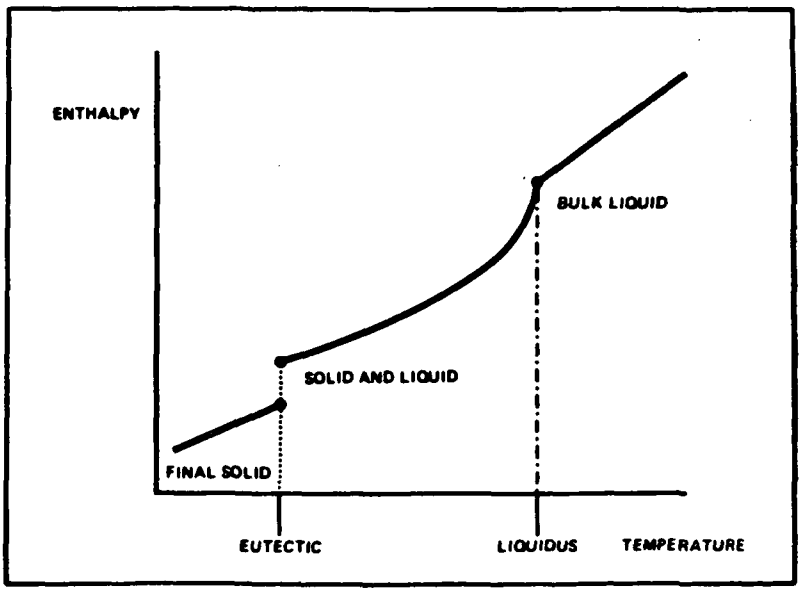

Figure 3-2. Temperature-Enthalpy Relationship for an Alloy with a Eutectic

In Fig. 3.2, the curvature in the mushy zone is caused by the dependence of the specific heat on the local fraction liquid. There is a jump discontinuity at the eutectic temperature due to the release of the latent heat of solidification of the eutectic phase, and a corner at the liquidus temperature due to a discontinuity in the specific heat of the material.

The form of the heat flux vector depends on the active heat transfer processes in each zone. In the liquid region, there is heat flow due to conduction as well as convection,

$$\vec{\Phi} = \rho_L H_L \vec{v} - k_T(T)\nabla T \ , \qquad (3.1.9)$$

where the form of the thermal conductivity k_T is given in Appendix A for each alloy, and the remaining variables are defined in Section 2. In the mushy zone, the heat flux has a convective term due to the interdendritic fluid flow as well as a conductive term,

$$\vec{\Phi} = g_L \rho_L H_L \vec{v} - k_T(T, g_L)\nabla T \ , \qquad (3.1.10)$$

where the thermal conductivity takes into account the relative amounts of solid and liquid phase material. In the solid region, the heat flux is due to conduction only, but the conductivity does depend on the amount of eutectic phase present; thus

$$\vec{\Phi} = - k_T(T, g_E)\nabla T \ . \qquad (3.1.11)$$

Boundary conditions must be specified at all external boundaries. The normal flux is zero at all insulated walls,

$$\partial T/\partial x = 0 \text{ and } \Phi_x = 0 \text{ on } x = X \text{ for } 0 \leq y \leq Y \text{ , and} \qquad (3.1.12)$$

$$\frac{\partial T}{\partial y} = 0 \text{ and } \Phi_y = 0 \text{ on } y = 0 \text{ and } y = Y \text{ for } 0 \leq x \leq X \text{ , } \qquad (3.1.13)$$

where Y is the dimension of the casting parallel to the chill face and X is the distance from the chill to the center line or to the end wall. At the chill there is some interface resistance so that the surface temperature of

the casting varies with time, and the heat flux is parameterized by both the heat transfer coefficient and the temperature of the chill:

$$\Phi_x = -\, h(T-T_{chill}) \qquad \text{on } x = 0 \quad \text{for } 0 \leq y \leq Y \quad . \tag{3.1.14}$$

The temperature of the chill, T_{chill}, is constant.

At each moving boundary there are two boundary conditions because the position of the boundary must also be determined. At the liquidus isotherm, the model allows no undercooling so that solid formation begins at the liquidus temperature and the heat flux through the isotherm is continuous; therefore

$$\left.\begin{aligned} T &= T_{LO} \\ \left[\vec{\Phi}_M - \vec{\Phi}_L\right]\cdot\vec{n}_{\Sigma L} &= 0 \end{aligned}\right\} \quad \text{on } x = x_L(t,y) \tag{3.1.15}$$

where $\vec{\Phi}_M$ is the flux from the mushy side, $\vec{\Phi}_L$ is the flux to the liquid side and $\vec{n}_{\Sigma L}$ is the local normal to the liquidus isotherm. At the eutectic front the difference in heat fluxes across the interface is given by the latent heat released upon solidification of the eutectic constituent times the rate of movement of the interface normal to itself:

$$\left.\begin{aligned} T &= T_E \\ \left[\vec{\Phi}_S - \vec{\Phi}_M\right]\cdot\vec{n}_{\Sigma E} &= U_{\Sigma E}\left[\overline{(\rho H)}^*_S - \overline{(\rho H)}^*_M\right] \end{aligned}\right\} \quad \text{on } x = x_E(t,y) \tag{3.1.16}$$

where $\overline{(\rho H)}^*_S$ is the enthalpy at the solid side of the interface and $\overline{(\rho H)}^*_M$ is the enthalpy at the S/L side of the interface.

The boundary conditions at the liquidus are called "implicit" because they do not reference the position or rate of movement of the boundary. The conditions at the eutectic are called "explicit" because $U_{\Sigma E}$, the rate of movement of the boundary, appears in the second condition.

3.1.3 Interdendritic Fluid Flow

The interdendritic fluid flow in the S/L region is described by the equations for total-mass and solute-mass conservation together with Darcy's Law for flow through a porous medium. The analysis leading to the conservation equations is based upon the concept of a volume element or cell within the S/L zone which is small enough to be treated as a differential element, yet large enough so that the volume fraction solid within it is equal to its local average value. This volume element concept is developed in Ref. 3. There is no solid phase movement into or out of the cell; there is no diffusive mass flux into or out of the cell; and the temperature and liquid density vary only differentially across the cell. With these assumptions, conservation of total mass within the volume element is written.

$$\frac{\partial}{\partial t}\left(\rho_S g_S + \rho_L g_L\right) = -\nabla \cdot \rho_L g_L \vec{v} \ . \qquad (3.1.17)$$

(See Section 2 for definitions of the symbols.) If solute enters or leaves the cell only by liquid convection, if there is no solute diffusion within the solid phase, and if the composition of the liquid within the volume element is uniform, then conservation of solute in the volume element is written

$$\frac{\partial}{\partial t}\left(C_S \rho_S g_S + C_L \rho_L g_L\right) = -\nabla \cdot C_L \rho_L g_L \vec{v} \ , \qquad (3.1.18)$$

where C_S is the local average solid composition defined by

$$\frac{\partial}{\partial t}\left(C_S \rho_S g_S\right) = k C_L \rho_S \frac{\partial g_S}{\partial t} \ . \qquad (3.1.19)$$

Darcy's Law for flow through a porous medium is used to relate the interdendritic fluid velocity directly to pressure. Thus

$$\vec{v} = -\frac{K}{\mu g_L}\left(\nabla p + \rho_L \vec{g}\right) \ , \qquad (3.1.20)$$

where μ is the viscosity of the liquid. The permeability, K, is a local function of solidification time and fraction liquid as described in Ref. 11.

Mass fluxes at the edges of the S/L zone provide boundary conditions for the conservation equations. The top and bottom of the S/L zone are in contact with the mold walls so that there is no normal component of flow; then

$$v_Y = 0 \quad \text{at} \quad y = 0 \quad \text{and} \quad y = Y \quad \text{for} \quad x_E \leq x \leq x_L \; . \tag{3.1.21}$$

As described in Ref. 1, flow at the eutectic isotherm must compensate for solidification shrinkage or expansion of the eutectic phase:

$$\rho_{LE} \vec{v} \cdot \vec{n}_{\Sigma E} + (\rho_{SE} - \rho_{LE}) U_{\Sigma E} = 0 \quad \text{on} \quad x = x_E \quad \text{for} \quad 0 \leq y \leq Y \tag{3.1.22}$$

where $\vec{n}_{\Sigma E}$ is the local unit normal to the eutectic isotherm and $U_{\Sigma E}$ is the speed of the isotherm in the $\vec{n}_{\Sigma E}$ direction. It is assumed that there is no convection in the bulk liquid, so that

$$p = p_0 + \rho_L g_L \, (Y-y) \quad \text{at} \quad x = x_L \quad \text{for} \quad 0 \leq y \leq Y. \tag{3.1.23}$$

In addition, at the liquidus isotherm the volume fraction liquid is given by

$$g_L = 1 \quad \text{at} \quad x = x_L \quad \text{for} \quad 0 \leq y \leq Y \; . \tag{3.1.24}$$

During the initial transient, the left boundary of the S/L zone is in contact with the chill face of the mold and Eq. (3.1.22) is replaced by the condition of zero normal mass flux:

$$v_X = 0 \quad \text{at} \quad x = 0 \quad \text{for} \quad 0 \leq y \leq Y \; . \tag{3.1.25}$$

During the final transient, the right boundary of the S/L zone is at the mold centerline or wall and Eq. (3.1.23) is applied.

In the previous solidification models (Refs. 9-11) a "local solute redistribution equation" and a "pressure equation" were derived from the flow equations for use in obtaining a numerical solution. In the current model, finite differences are applied directly to the equations obtained by substituting Eq. (3.1.19) and Eq. (3.1.20) into Eq. (3.1.17) and Eq. (3.1.18). Details of the numerical analysis are presented in Section 3.2.

3.1.4 Macrosegregation

After solidification is complete at a point (x,y) in the casting, the final local average composition is given by

$$\bar{C}_S(x,y) = \left[\rho_S \int_{g_S=0}^{1-g_E} kC_L dg_S + \rho_{SE} g_E C_E\right] \Big/ \left[\rho_S(1-g_E) + \rho_{SE} g_E\right] \qquad (3.1.26)$$

The integral term accounts for the solute within the dendritic solid, and the second term in the numerator accounts for the solute in the eutectic constituent.

3.2 Numerical Methods

3.2.1 Introduction

The description of heat flow during the solidification of an alloy is a moving boundary problem with two moving internal boundaries which define a region of both solid and liquid phases. The boundaries of this region are associated with discontinuities in the functional relationship between temperature and enthalpy, and a numerical solution of the energy equation in the presence of such discontinuities requires special techniques. This section describes a new method of implementing the boundary conditions that allows an accurate and smooth determination of the internal boundary locations where this information is critical as in predicting the flow field within the S/L region.

3.2.1.1 Problem Description

A moving boundary problem is an initial value problem described by a system of parabolic partial differential equations with one or more boundaries which move in a way that depends on the solution of the differential equations (13). There are two boundary conditions to be satisfied for each moving boundary because its position is unknown a priori. Moving boundary problems are nonlinear problems: the position of the boundary must be determined simultaneously with the solution of the partial differential equations.

There are two types of boundary conditions at a moving boundary. The most common is the "explicit" (13) condition where one or both of the boundary

conditions explicitly specifies the velocity of the boundary. In a problem with an "implicit" condition, neither boundary condition specifies the velocity of the boundary. As shown below, the boundary conditions at the eutectic isotherm are explicit while those at the liquidus isotherm are implicit. This poses an especially difficult numerical problem because most existing techniques that work for explicit boundary conditions do not apply to implicit boundary conditions, and techniques designed for problems with implicit boundary conditions rely on analytical manipulations that are not feasible for problems as complex as the macrosegregation calculation (14,15). The exception to this is the "enthalpy technique" (16,17) which is discussed below.

There is another aspect of the macrosegregation calculation which makes it a particularly difficult moving boundary problem. The solution to the macrosegregation equations is especially sensitive to the rate of movement of the mushy zone both because the boundary condition at the eutectic is in terms of the velocity of that boundary and because the movement of the entire mushy zone must be accounted for by the numerical technique used to solve the conservation equations. Thus slight inaccuracies, especially fluctuations, in the calculated rate of movement of the boundaries cause substantial errors and a failure to obtain convergence in the solution of the macrosegregation equations.

3.2.1.2 Development of a Solution Technique

In recent years a great variety of numerical techniques have been developed to solve moving boundary problems. A review can be found in Ref. 13. Existing techniques were bound to be unsuitable because one or both of the following features could not be treated adequately:

a. the position and rate of movement of the boundaries are crucial to the calculation and, therefore, must be accurately determined, and
b. there is no explicit boundary condition at the liquidus interface.

Techniques for moving boundary problems can be differentiated by their treatment of the computational node points. Fixed-grid techniques carry out the calculations on a grid that is stationary in the physical domain, using special interpolation formulas in the cells containing the moving boundary.

Variable space-grid techniques operate on grids that deform as each subregion changes. The Murray-Landis method (18) and applications of finite element methods (19) are examples of variable grid techniques. Coordinate transformation techniques actually transform the equations to a domain where the moving boundaries are fixed for all time; the calculation is carried out on the fixed grid in the transformed domain. The enthalpy method (16,17) deserves special attention because it has been successfully applied to solving many moving boundary problems. It can be used to solve an integral form of the energy equation on a grid that is fixed in the physical domain without reference to the locations of the moving boundaries.

Previous applications of all these techniques except the enthalpy method require explicit boundary conditions to follow the boundary movement, and thus they are not applicable without modification at the liquidus interface. The enthalpy method was tested extensively for use in this problem, but with it, the positions and velocities of the moving boundaries could not be determined with sufficient accuracy to give sensible results for the macrosegregation calculation. Because of these difficulties, it was necessary to devise a new method of applying the boundary conditions.

3.2.2 Discrete Flux Method

The philosophy of the discrete flux method is to preserve the physical conservation relations both analytically and in discrete form. In effect, the finite difference equations "simulate" heat flow through the discrete computational mesh. The resulting discrete form of the moving boundary conditions is explicit whether the original analytical form is explicit or implicit.

The approach is first to transform the equations to body-fitted curvilinear coordinates, retaining both enthalpy and temperature as dependent variables. Then write conserving finite difference approximations for each of the interior and boundary coordinates. Finally, obtain conditions which determine the movement of the internal boundaries such that the correct discrete heat flux relations are maintained at the interfaces. This last step is the one that distinguishes the discrete flux method from other techniques.

3.2.2.1 Coordinate Transformation

Each of the three regions is transformed to a unit square as shown in Fig. 3.3. The moving boundaries are now included among edges of the squares. A computational mesh is set up in each of the three squares with horizontal mesh widths $\Delta\xi_S$, $\Delta\xi_M$, $\Delta\xi_L$ and vertical mesh width $\Delta\eta$ for all regions. The uniform vertical mesh spacing insures that points in adjacent regions coincide along the edges corresponding to the internal moving boundaries.

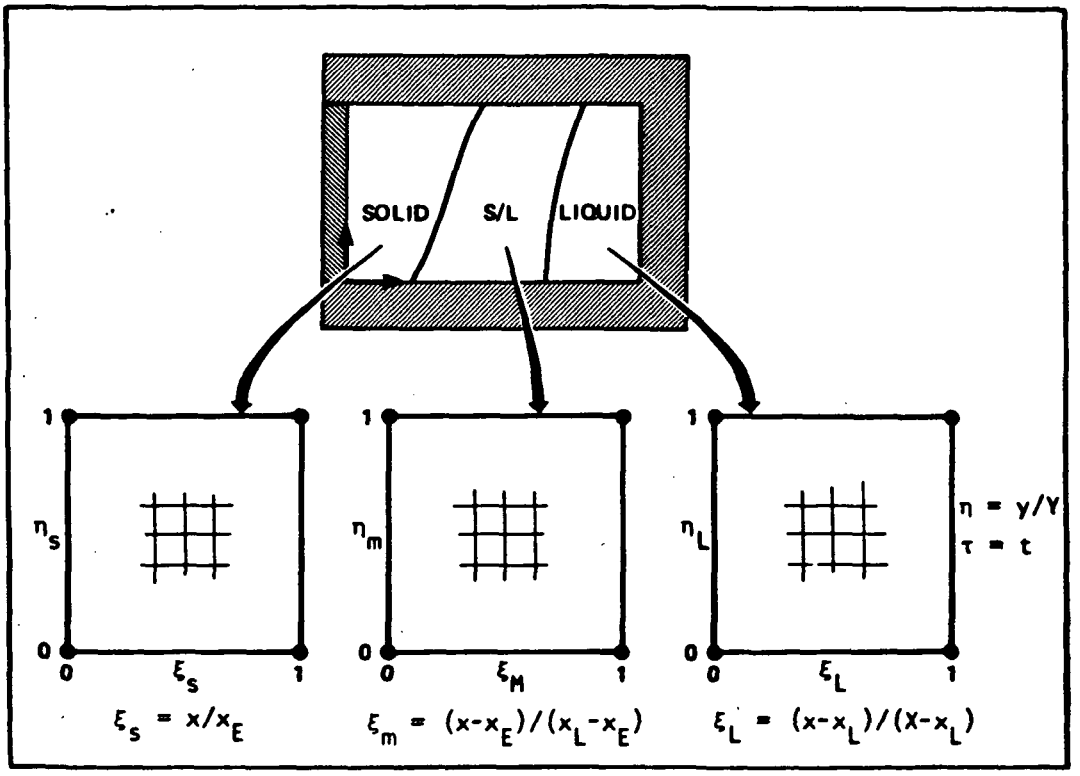

Figure 3-3. The Coordinate Transformation

Following the methods of Thompson et al. (20) and Viviand (21), the energy equation for each region is transformed to the computational space and the resulting equation is rewritten in conservation law form.

$$\frac{\partial \overline{\rho H}}{\partial t} = -\left(\frac{\partial \Phi_x}{\partial x} + \frac{\partial \Phi_y}{\partial y}\right) \rightarrow \frac{\partial}{\partial \tau}(J\overline{\rho H}) = -\left(\frac{\partial F}{\partial \xi} + \frac{\partial G}{\partial \eta}\right) \qquad (3.2.1)$$

$$\text{where } F = -y_\eta x_\tau \overline{\rho H} + y_\eta \Phi_x - x_\eta \Phi_y \quad \text{and} \qquad (3.2.2)$$

$$G = x_\xi \phi_y \quad . \tag{3.2.3}$$

$J = x_\xi y_\eta$ is the Jacobian determinant of the transformation and x_ξ, x_η, x_τ and y_η are coefficients of the transformation that depend on the size and rate of deformation of the corresponding physical region (16). In Eqs. (3.2.1)-(3.2.3), F and G are the heat fluxes in the ξ- and η- directions, respectively. The first term in F is due to the movement of the physical domain; x_τ is the local rate of movement.

The mass conservation equations are of the same form as the energy equations and they transform in the same way. The total mass conservation equation transforms to

$$\frac{\partial \bar{\rho}}{\partial t} = -\nabla \cdot (\rho_L g_L \vec{v}) \rightarrow \frac{\partial}{\partial \tau}(J\bar{\rho}) = -\left(\frac{\partial F_M}{\partial \xi} + \frac{\partial G_M}{\partial \eta}\right) \tag{3.2.4}$$

where
$$\bar{\rho} = \rho_S g_S + \rho_L g_L \ , \tag{3.2.5}$$

$$F_M = -y_\eta x_\tau \bar{\rho} + \rho_L g_L (y_\eta v_X - x_\eta v_Y), \text{ and} \tag{3.2.6}$$

$$G_M = \rho_L g_L (x_\xi v_Y) \ . \tag{3.2.7}$$

F_M and G_M are mass fluxes in the ξ- and η- directions, respectively, relative to the fixed (ξ, η) coordinates due both to convection of the interdendritic liquid and to deformation of the physical (x,y) domain. The solute mass conservation equation, Eq. (3.1.18), is slightly complicated by the substitution of Eq. (3.1.19).

$$-\hat{\rho} \frac{\partial C_L}{\partial t} + \frac{\partial}{\partial t}(\hat{\rho} C) = -\nabla \cdot (\rho_L g_L C_L \vec{v}) \tag{3.2.8}$$

where
$$\hat{\rho} = \rho_S g_S k \quad \text{and} \quad \hat{\rho} C = \rho_L g_L C_L + \rho_S g_S k C_L \ . \tag{3.2.9}$$

Eq. (3.2.8) transforms to

$$-\hat{\rho}\left[\frac{\partial}{\partial \tau}(JC_L) + \frac{\partial}{\partial \xi}(F_C)\right] + \frac{\partial}{\partial \tau}(J\hat{\rho}C) = -\left(\frac{\partial F_S}{\partial \xi} + \frac{\partial F_S}{\partial \eta}\right) \tag{3.2.10}$$

where

$$F_C = - y_\eta x_\tau C_L \ , \tag{3.2.11}$$

$$F_S = - y_\eta x_\tau \hat{\rho} C + \rho_L g_L C_L (y_\eta v_X - x_\eta v_Y), \text{ and} \tag{3.2.12}$$

$$G_S = \rho_L g_L C_L (x_\xi v_Y) \ . \tag{3.2.13}$$

3.2.2.2 Finite Difference Approximations to the Energy Equation

In order to write conserving finite difference expressions, the energy equation is integrated over each cell in the computational mesh, and Green's theorem is applied to give

$$\iint_{\text{cell}} \frac{\partial}{\partial \tau}(J\overline{\rho H})\, d\xi d\eta = - \oint_{\substack{\text{cell} \\ \text{boundary}}} F d\eta - G d\xi \ . \tag{3.2.14}$$

Thus, the difference equations can be written in terms of fluxes through the cell walls.

3.2.2.2.1 Interior and Wall Cells

The (i,j) interior cell and the (1,j) wall cell are illustrated in Fig. 3.4. The following discussion applies to all regions. Note that the heat fluxes are defined to be positive in the direction of increasing ξ or η. Assuming that the function values at the node points represent the function throughout the cell and applying Eq. (3.2.14) to the interior cell gives

$$\frac{1}{\Delta\tau}(J\overline{\rho H}^{n+1} - J\overline{\rho H}^{n})_{ij} \Delta\eta\Delta\xi = (F_{in} - F_{out})^{n+1}_{\Delta\eta} + (G_{in} - G_{out})^{n+1}_{\Delta\xi} \ . \tag{3.2.15}$$

F_{in} and F_{out} are obtained by evaluating Eq. (3.2.2) at $i-\frac{1}{2}$ and $i+\frac{1}{2}$ respectively, where for example,

$$(\phi_x)_{i+\frac{1}{2},j} = -k(1/x_\xi)(T_{i+1,j} - T_{i,j}) \ /\Delta\xi, \text{ and} \tag{3.2.16}$$

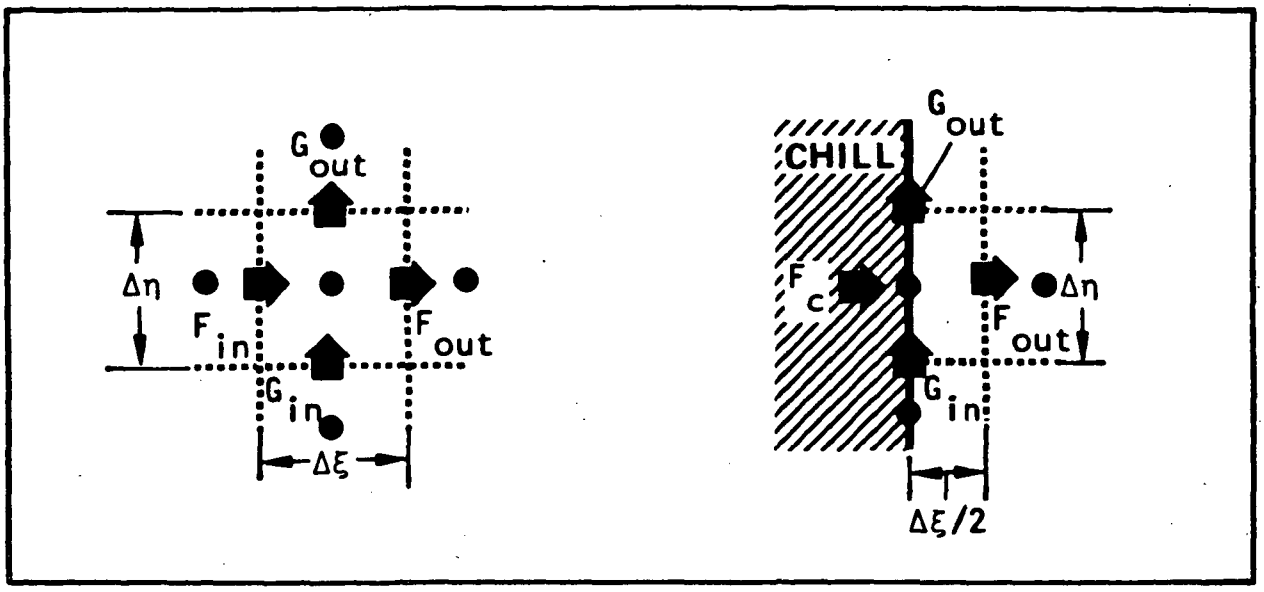

Figure 3.4 - Schematic of Heat Fluxes at the Interior and Wall Cells

$$(\phi_y)_{i+\frac{1}{2},j} = -k\left[-(x_\eta/x_\xi y_\eta)(T_{i+1,j} - T_{i,j})/\Delta\xi + \tfrac{1}{2}(1/y_\eta)(T_{ij+1} - T_{ij-1} + T_{i+1j+1} - T_{i+1j-1})/2\Delta\eta\right] \quad (3.2.17)$$

When fully expanded, Eq. (3.2.15) is identical to a space-centered finite difference approximation. The equation for the wall cell is similar except for the difference in cell size; accordingly

$$\frac{1}{\Delta\tau}(J\overline{\rho H}^{n+1} - J\overline{\rho H}^{n})_{1j}\Delta\eta\Delta\xi/2 = (F_c - F_{out})^{n+1}_{\Delta\eta} + (G_{in} - G_{out})^{n+1}_{\Delta\xi/2} \; . \quad (3.2.18)$$

3.2.2.2.2 Interface Cells

There remain to be defined the computational expressions for determining the movement of the internal interfaces or moving boundaries. These will be

derived by applying the method used for the interior cells and the wall cells to the cells situated at the moving internal boundaries and then by using the moving boundary conditions to resolve the unknown fluxes.

Figure 3.5 illustrates cells at the internal moving boundaries of the computational mesh. The cell on the left is in the solid region and the cell on the right is in the mushy zone. When mapped back to physical space, the boundary node points from each cell coincide and lie on the eutectic isotherm.

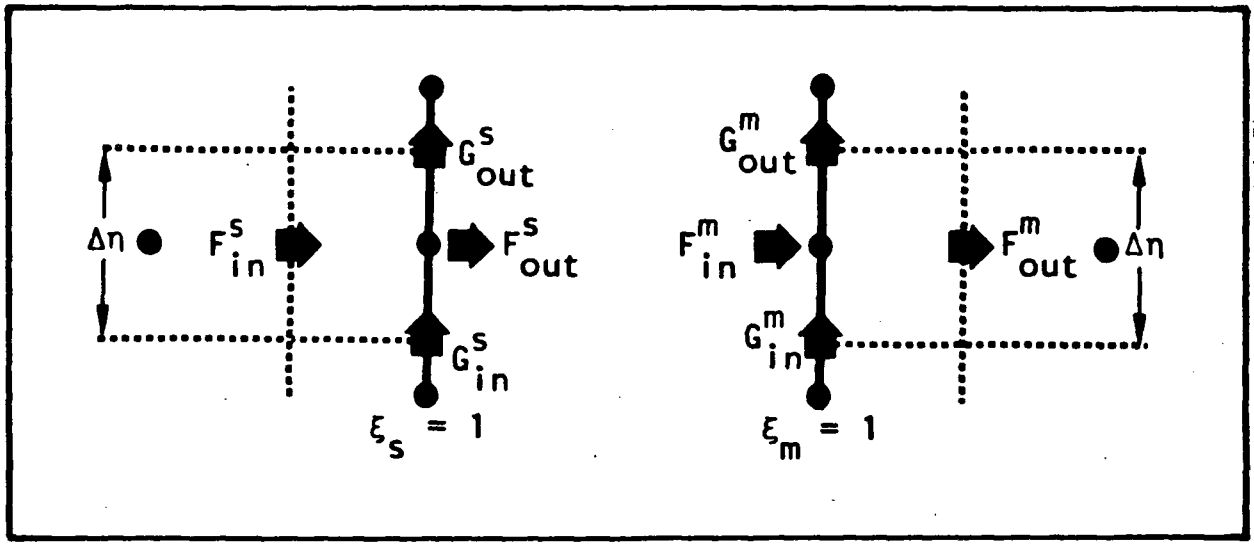

Figure 3-5. Schematic of Heat Fluxes at Cells in the Solid and Mushy Regions along the Eutectic Interface Boundary.

Applying Eq. (3.2.14) to the cell in the mapped solid region leads to

$$\frac{1}{\Delta\tau}(J\overline{\rho H}_s^{n+1} - J\overline{\rho H}_s^{n})_{N,j}\Delta\eta\Delta\xi_s/2 = (F^s_{in} - F^s_{out})^{n+1}_{\Delta\eta} + (G^s_{in} - G^s_{out})^{n+1}_{\Delta\xi_s}/2 \quad , (3.2.19)$$

where the subscript S means the quantity is evaluated in the solid region. In this case $\overline{\rho H}_S^{n+1}$ is known as a result of the first of Eqs. (3.1.16), and the temperature-enthalpy relationship, but F^s_{out} is considered to be unknown. Similarly, the energy conservation equation applied to the cell in the mushy region leads to

$$\frac{1}{\Delta\tau}(J\overline{\rho H}_M^{n+1} - J\overline{\rho H}_M^{n})_{1,j}\Delta\eta\Delta\xi_M/2 = (F^M_{in} - F^M_{out})^{n+1}_{\Delta\eta} + (G^M_{in} - G^M_{out})^{n+1}_{\Delta\xi_M}/2 \quad , (3.2.20)$$

where the subscript M means the quantity is evaluated in the mushy region. Again, $\overline{\rho H}_M^{n+1}$ is known, but F_{in}^M is unknown. The second moving boundary condition at the eutectic isotherm provides another relationship between the unknown fluxes; the relationship is

$$y_\eta \, x_\tau (\overline{\rho H}_s^{n+1} - \overline{\rho H}_M^{n+1}) = F_{out}^s - F_{in}^M \quad . \qquad (3.2.21)$$

The two unknown fluxes are eliminated algebraically from Eqs. (3.2.19), (3.2.20), and (3.2.21), and the resulting equation is used to determine the rate of boundary movement by solving for x_τ. The same procedure is applied at the liquidus interface. In this case x_τ does not appear in the interface condition analogous to Eq. (3.2.21), but it does appear in the remaining ξ-fluxes, F_{in}^M and F_{out}^L, so that the final condition at the liquidus boundary is explicit even though the original form of the boundary condition in real space and time is implicit.

In effect the rate of the internal boundary movement is determined so as to satisfy both the energy conservation equations in the cells adjacent to the boundary and the condition at the moving boundary itself. The equations are well posed for determining the boundary movement so long as temperature and enthalpy are not uniform throughout all adjacent cells.

3.2.2.3 Finite Difference Approximations to the Mass Conservation Equations

The derivation of the finite difference approximations for the mass conservation equations parallels that for the energy equation. The equations are integrated over each computational cell, Green's theorem is applied to the divergence terms, and then the finite differences are written in terms of mass fluxes through the cell walls. For example, the total mass conservation Eq. (3.2.4), written as a difference equation in the interior cell shown at the left of Fig. 3.4 is

$$\frac{1}{\Delta\tau} (J\bar{\rho}^{n+1} - J\bar{\rho}^{n})_{ij} \, \Delta\eta\Delta\xi = (F_{M(in)} - F_{M(out)})_{\Delta\eta}^{n+1} + (G_{M(in)} - G_{M(out)})_{\Delta\xi}^{n+1} \quad . \qquad (3.2.22)$$

In order to apply finite differences to the mass flux terms, the expressions containing velocity in Eq. (3.2.6) and Eq. (3.2.7) must be expanded in terms of pressure by substituting Darcy's Law, Eq. (3.1.20); this yields

$$F_M = - y_\eta x_\tau \bar{\rho} - \rho_L \frac{K}{\mu} \left\{ C_{\xi\xi} \frac{\partial p}{\partial \xi} + C_{\xi\eta} \frac{\partial p}{\partial \eta} + (\rho_L - \rho_{L0})(y_\eta g_x - x_\eta g_y) \right\} \quad (3.2.23)$$

where $$C_{\xi\xi} = (y_\eta^2 + x_\eta^2)/x_\xi y_\eta \quad \text{and} \quad C_{\xi\eta} = - x_\eta / y_\eta \ , \text{ and} \quad (3.2.24)$$

$$G_M = - \rho_L \frac{K}{\mu} \left\{ C_{\xi\eta} \frac{\partial p}{\partial \xi} + C_{\eta\eta} \frac{\partial p}{\partial \eta} + (\rho_L - \rho_{L0})(x_\xi g_y) \right\} \quad (3.2.25)$$

where $$C_{\eta\eta} = x_\xi / y_\eta \ . \quad (3.2.26)$$

Then finite differences are substituted for the pressure derivatives:

$$\left(\frac{\partial p}{\partial \xi} \right)_{i \pm \frac{1}{2}, j} \approx \pm (p_{i \pm 1, j} - p_{i,j})/\Delta\xi \ , \quad (3.2.27)$$

$$\left(\frac{\partial p}{\partial \eta} \right)_{i \pm 1, j} \approx \frac{1}{2} (p_{i,j+1} - p_{i,j-1} + p_{i \pm 1, j+1} - p_{i \pm 1, j-1})/2\Delta\eta \ , \quad (3.2.28)$$

$$\left(\frac{\partial p}{\partial \xi} \right)_{i, j \pm \frac{1}{2}} \approx \frac{1}{2} (p_{i+1, j \pm 1} - p_{i-1, j \pm 1} + p_{i+1,j} - p_{i-1,j})/2\Delta\xi \ , \text{ and} \quad (3.2.29)$$

$$\left(\frac{\partial p}{\partial \eta} \right)_{i, j \pm \frac{1}{2}} \approx \pm (p_{i, j \pm 1} - p_{i,j})/\Delta\eta \ . \quad (3.2.30)$$

The remaining terms in Eqs. (3.2.23) and (3.2.25) are evaluated by suitable averages. The derivation of the equations for the boundary cells is similar. The type of boundary condition applied at each side of the S/L zone depends upon the stage of the solidification. During the initial transient, for example, the component of velocity normal to the left side is zero, and the transformed form of Eq. (3.1.25) must be substituted into the wall-cell form of Eq. (3.2.25). After the S/L zone is fully developed, the transformed form of Eq. (3.1.22) must be substituted into the wall-cell form of Eq. (3.2.25).

Finite difference approximations to the solute-mass conservation equation are derived in an analogous manner.

3.2.3 Solution of the System of Nonlinear Equations

The result of the analysis in the foregoing sections is a large system of nonlinear algebraic equations which give the temperature and enthalpy in all three zones as well as the volume fraction of liquid, velocity and pressure in the S/L zone, and the shape and rate of movement of the S/L zone. The system comprises equations which include the temperature-enthalpy relationships, Eqs. (3.1.2)-(3.1.8), the finite difference form of the energy equation in all three regions, the moving boundary conditions, Eqs. (3.2.19)-(3.2.21), the finite difference form of the total-mass conservation equation and the finite difference form of the solute-mass conservation equation. If the horizontal dimensions of the finite difference grid in the solid, mushy and liquid regions are N_S, N_M and N_L, respectively, then the number of unknowns to be determined at each time step and the number of coupled algebraic equations is

$$M = N_Y \left[2(N_S + N_M + N_L - 1) + 2\, N_M \right] \qquad (3.2.31)$$

where N_Y is the vertical dimension of the grid.

The system of equations is solved by the iterative Newton-Raphson method (22) for locating the zeros of a system of nonlinear equations. The recursive equation at each iteration is

$$X^{(k+1)} = X^{(k)} - J^{-1}\, Q(\vec{X}^{(k)}) \qquad (3.2.32)$$

where X is the vector of M unknowns, Q is the vector of functions whose zero is sought, and J is the Jacobian matrix of Q with respect to X.

For even a relatively coarse mesh the system of equations represented by Eq. (3.2.32) is quite large. For example, if there is a 10 x 10 grid in each region then M = 780 and an evaluation of Eq. (3.2.32) requires solution of a 780 x 780 matrix equation at each iteration. However, the structure of the equations in Q leads to a sparse partitioned structure for J which can be reduced analytically to the solution of a sequence of banded tridiagonal and pentadiagonal matrix equations, reducing the number of computer calculations immensely.

3.3 Program Results

3.3.1 One-Dimensional Results

For the purpose of developing and testing the numerical techniques for solving the moving boundary problem, a great deal of work was performed with a one-dimensional heat flow model. Some of the results are presented here.

3.3.1.1 Comparison of the Enthalpy Method to the Discrete Flux Method

Figure 3.6 illustrates the difficulty encountered in applying the enthalpy method (16, 17) to a one-dimensional macrosegregation calculation for an aluminum-copper alloy. Figures 3.6a and b are the position and rate of movement of the liquidus boundary as functions of time, and Fig. 3.6c and d are the position and rate of movement of the eutectic boundary as functions of time. The dotted lines were calculated by interpolating the temperature profile produced by the enthalpy method while the solid lines were calculated by the discrete flux method. The cusps in the liquidus time history from the enthalpy method are caused by the movement of the "corner" in the enthalpy-temperature function over the spatial mesh points. They appeared for all mesh spacings tested, up to an order of magnitude smaller than that shown in Fig. 3.6. The resulting rate of movement of the liquidus fluctuates discontinuously about the true value and actually becomes slightly negative at about 30 seconds.

The results for the movement of the eutectic boundary, Fig. 3.6c and d, are similar. In this case the fluctuations are caused by the movement of the step discontinuity over the nodes in the spatial mesh. Note that if the step in the enthalpy-temperature profile is replaced with a sloping line segment by the method described in Ref. (23), then there would be two corners near the eutectic, each with a behavior similar to that at the liquidus "corner."

Although the enthalpy method applies spatial finite differences across the mesh without regard to the location of the interface, the discontinuities and corners in the temperature-enthalpy relationship used to resolve the time-difference term of the difference equation are propagated as discontinuities in the spatial derivatives of enthalpy and temperature. Thus interpolating temperature or enthalpy to determine the location of the interface results in the type of temporal fluctuation shown in Fig. 3.6.

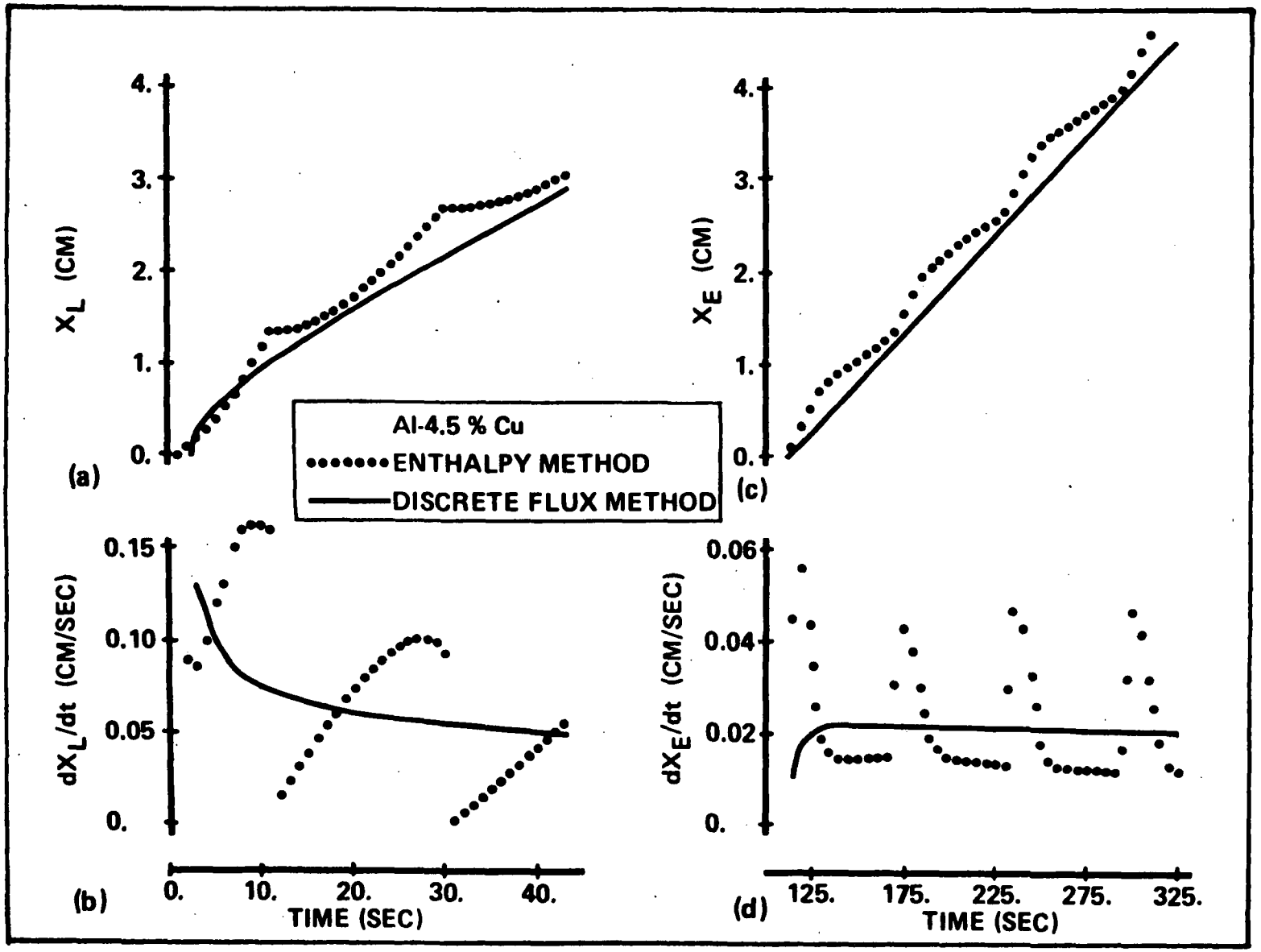

Figure 3.6. Interface Movement Calculated by the Enthalpy Method and by the Discrete Flux Method.

3.3.1.2 Comprison with Empirical Results

A one-dimensional theoretical result using the discrete flux method is compared with the experimental results of Koump et al (24) in Fig. 3.7. The heat transfer coefficient and the temperature at the chill were adjusted to produce the same average cooling rate at the chill and the same time for the liquidus to reach the end of the ingot. In Fig. 3.8 the same comparison is made for a slower cooling rate. Here only the temperature of the chill was adjusted to match the average cooling rate at the chill. Agreement between the calculated results and the measurements is reasonably good considering that the model used for the calculations assumes that heat transfer at the chill can be characterized by a constant and uniform heat transfer coefficient. In addition, perfect agreement between the calculated results and the experimental can not be expected because, for the three surfaces not chilled, perfect adiabaticity is assumed in the model whereas in the experiments such a boundary condition was only approximated.

3.3.2 Two-Dimensional Results

Figures 3.9-3.16 illustrate calculated results from the two-dimensional model used to compute temperature, composition and velocity in Al-4.5% Cu alloy as it solidifies. Temperature profiles across the casting at several times during the solidification are shown in Fig. 3.9. Any vertical variation in the temperature field is imperceptible on the scale of this plot. Figure 3.10 shows no vertical variation in the position of the eutectic isotherm, but a slight vertical slope develops in the liquidus isotherm as it progreses. This slope is primarily due to the combined effect of convective heat transfer in the S/L region and secondarily due to spatial variations in the thermal conductivity of the alloy caused by macrosegregation.

Figure 3.11 shows the final composition of the solid formed by the time the run was stopped at t = 451 seconds.

Figures 3.12-3.16 show the movement of the S/L zone across the mold, and within the S/L zone the vectors indicate the velocity of the interdendritic liquid. The S/L zone is bounded on the left and right by solid lines indicating the position of the eutectic and liquidus isotherms, respectively.

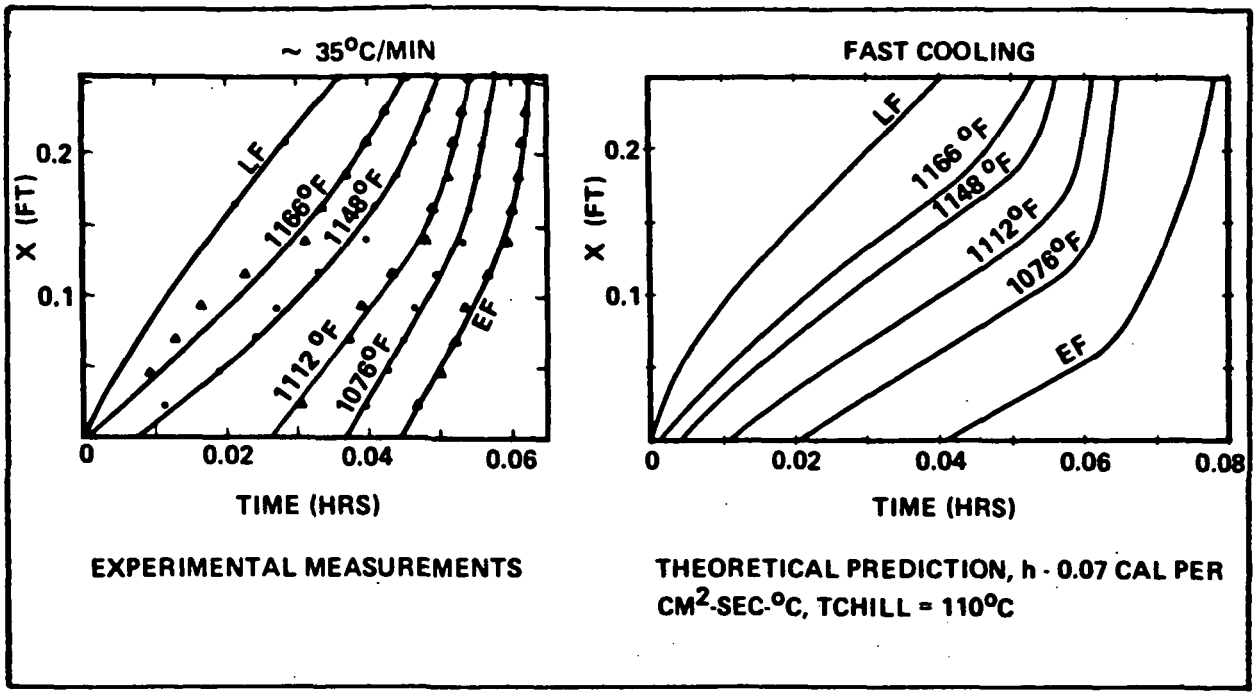

Figure 3.7. Comparison of the Experimental Measurements of Koump et al (24) with Model Prediction for Fast Cooling of A1-4.5% Cu.

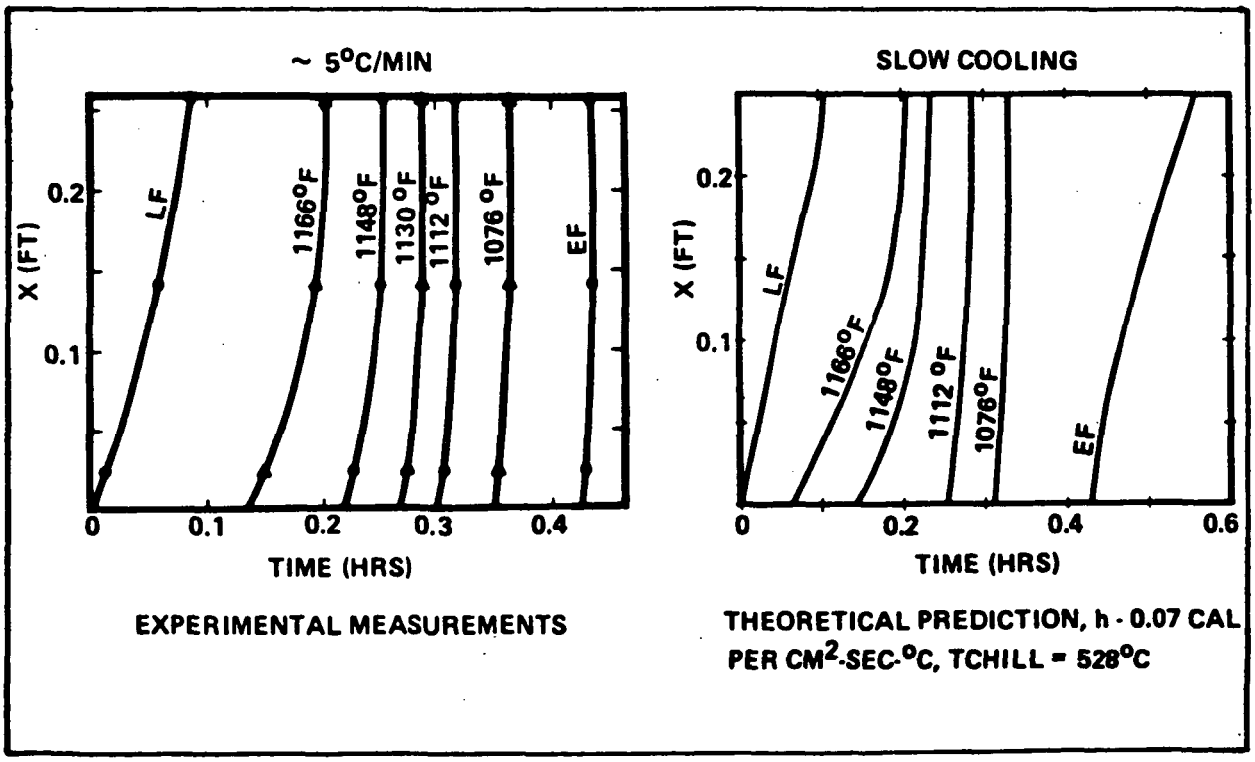

Figure 3.8. Comparison of the Experimental Measurements of Koump et al (24) with Model Prediction for Slow Cooling of A1-4.5% Cu.

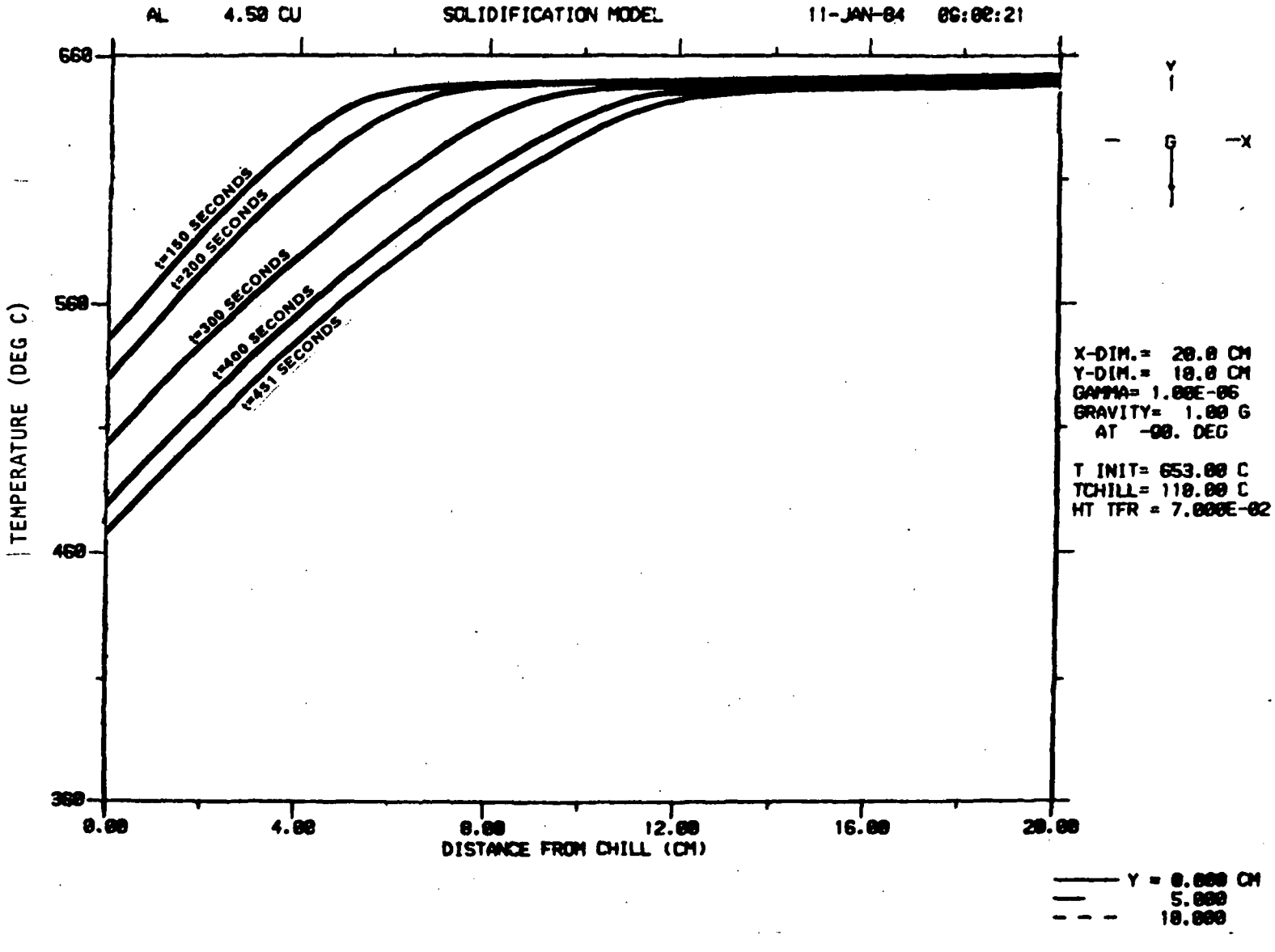

Figure 3.9. Time Varying Temperature Profiles Across the Casting

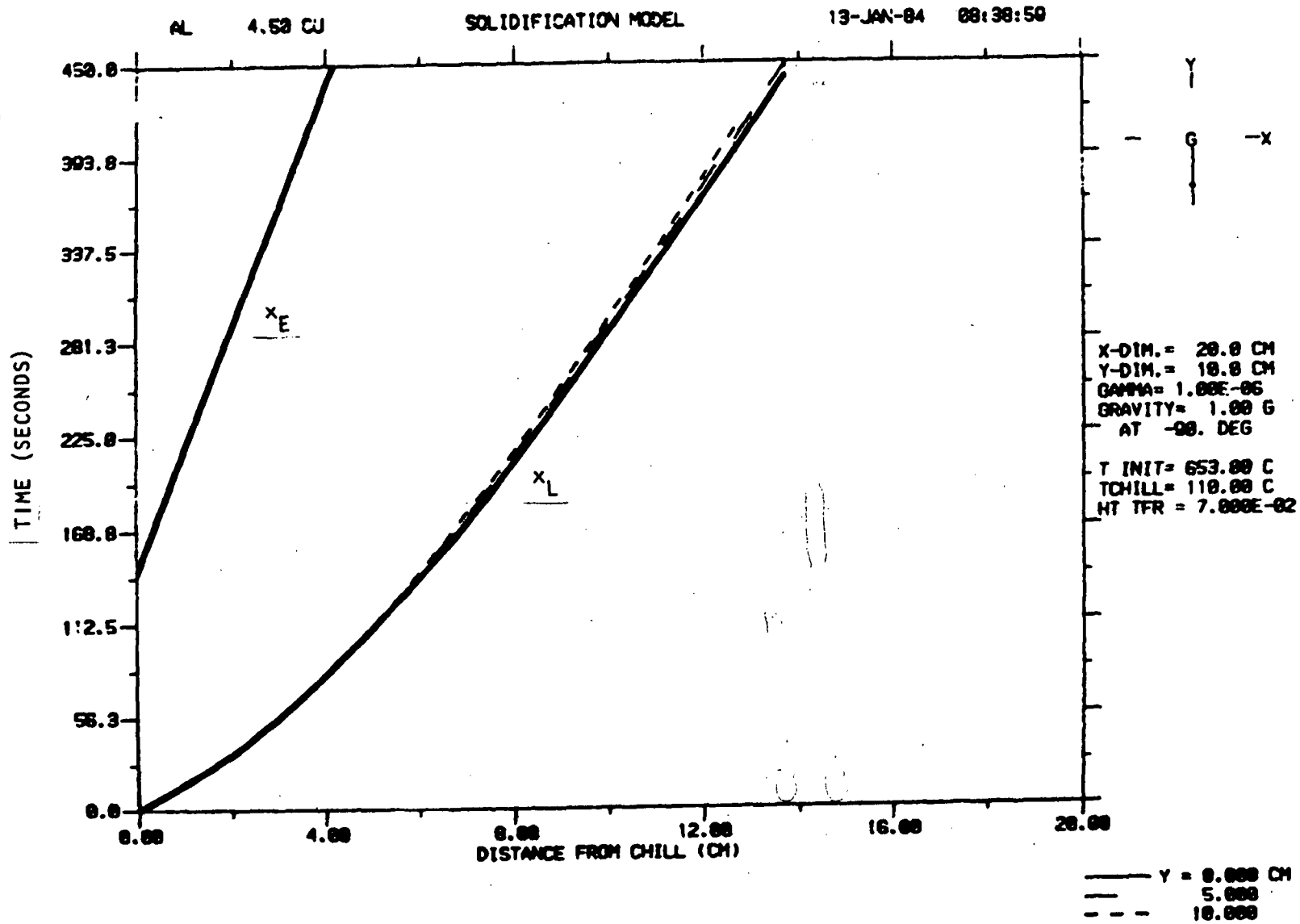

Figure 3.10. Movement of the Liquidus and Eutectic Isotherms

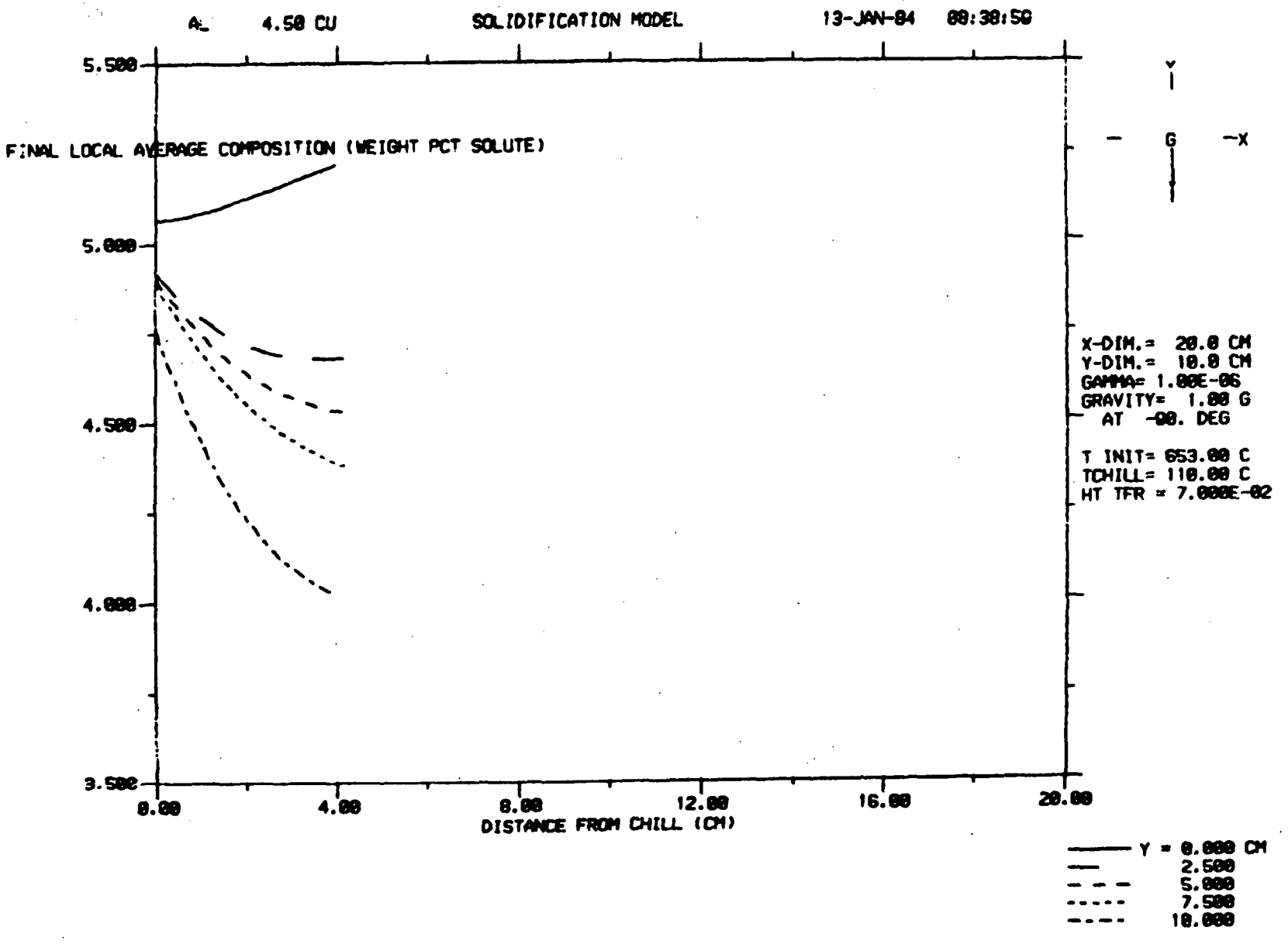

Figure 3.11. Final Composition in the Fully Solid Region

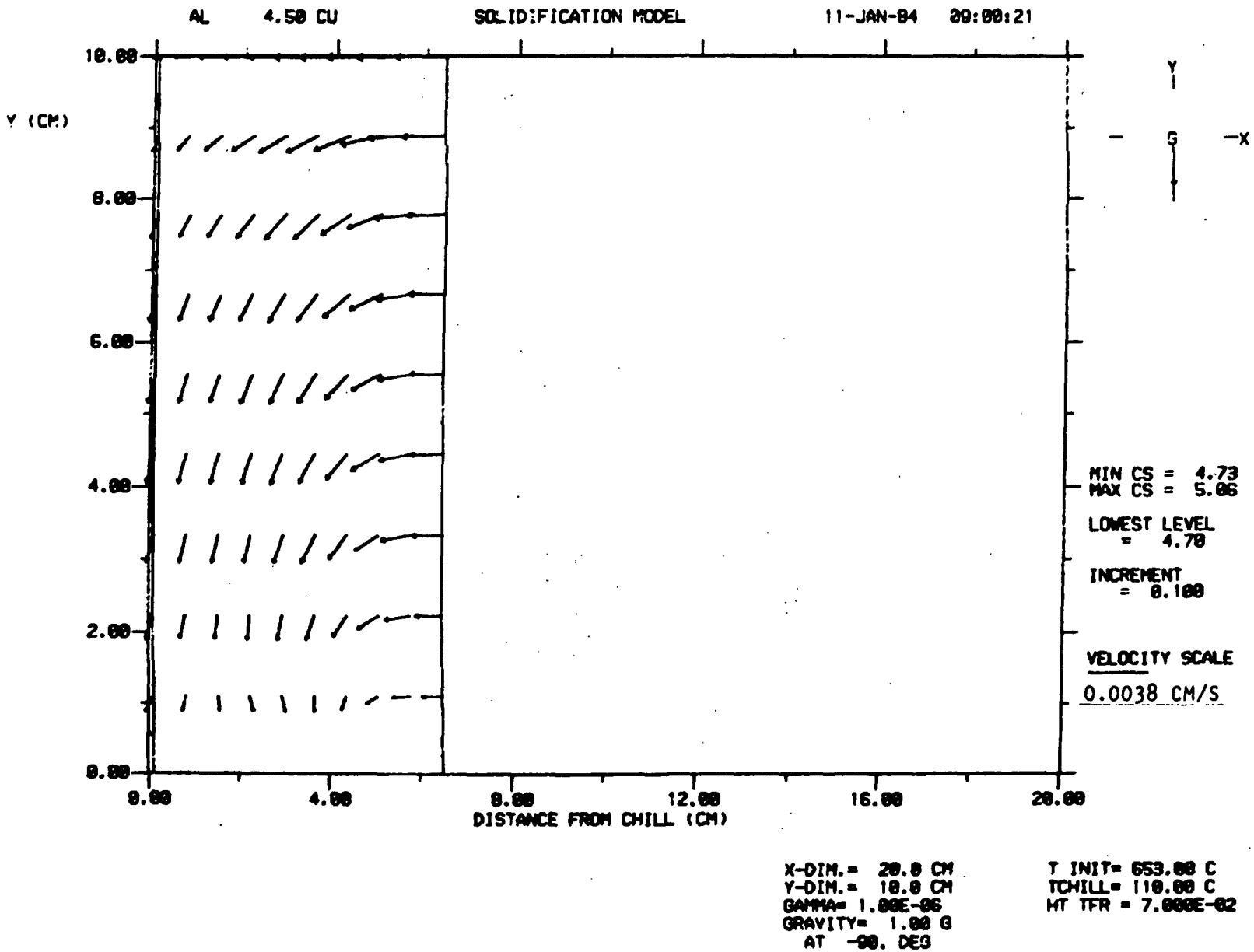

Figure 3.12. Final Local Average Composition and Interdendritic Fluid Velocity at t = 150 Seconds

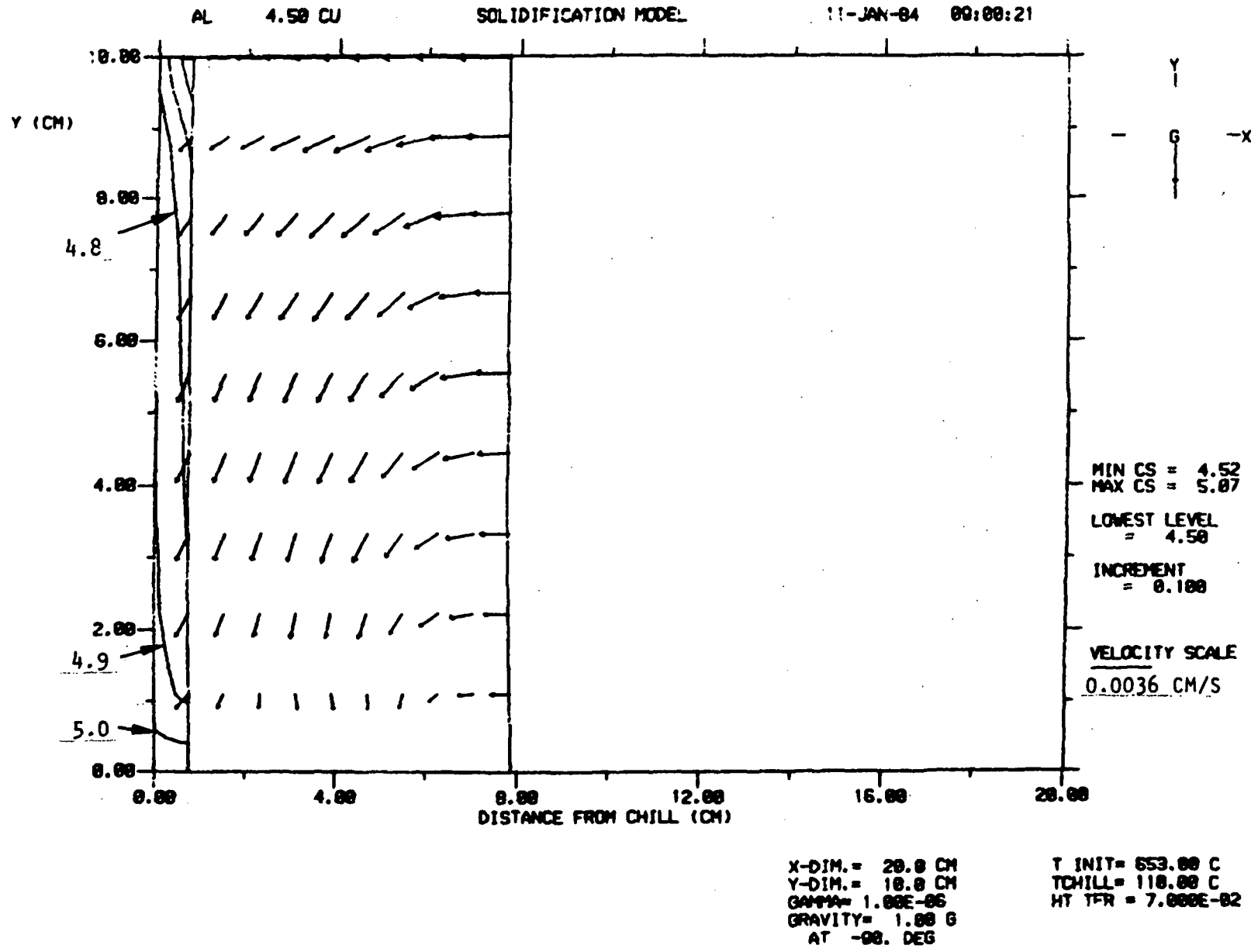

Figure 3.13. Final Local Average Composition and Interdendritic Fluid Velocity at t = 200 Seconds

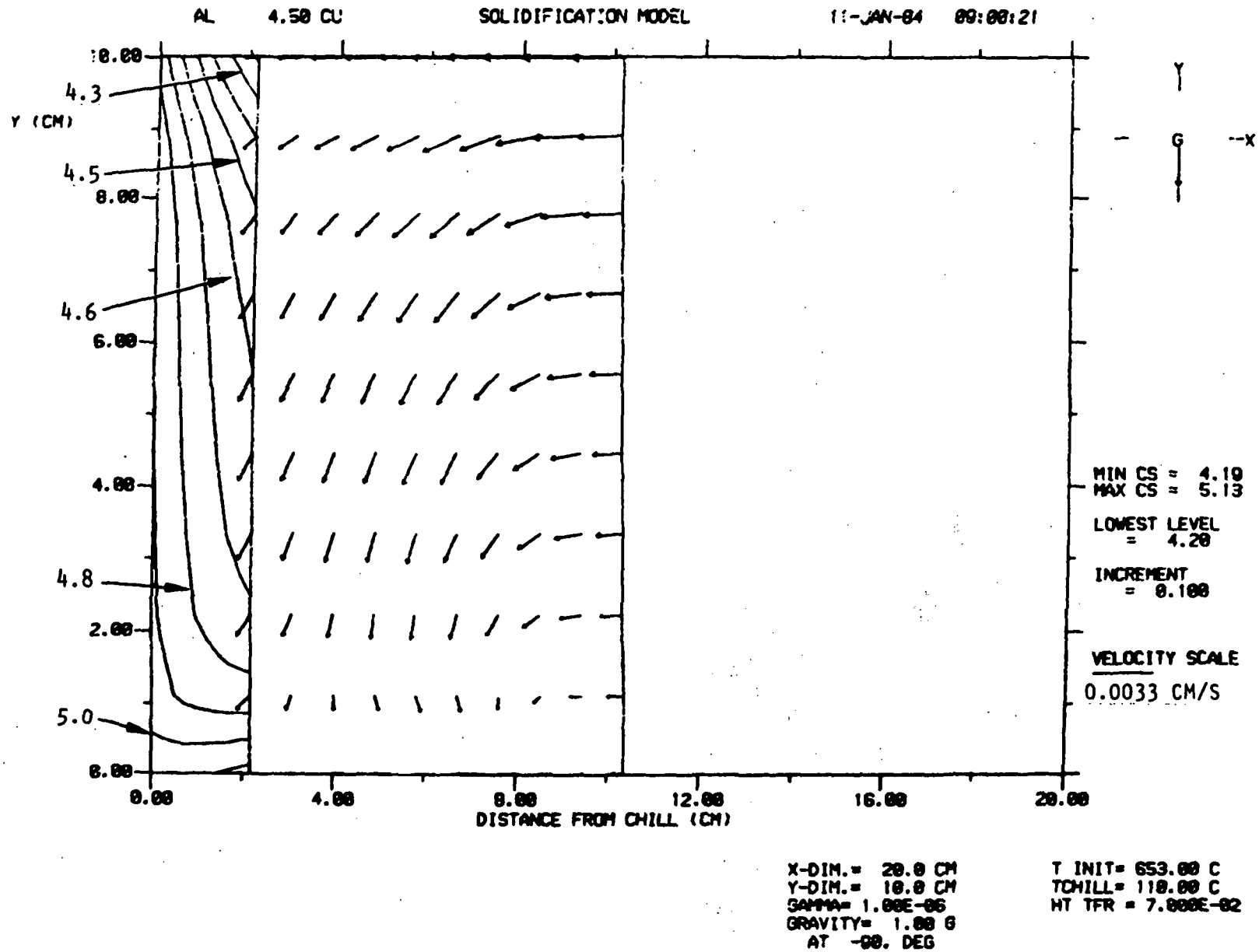

Figure 3.14. Final Local Average Composition and Interdendritic Fluid Velocity at t = 300 Seconds

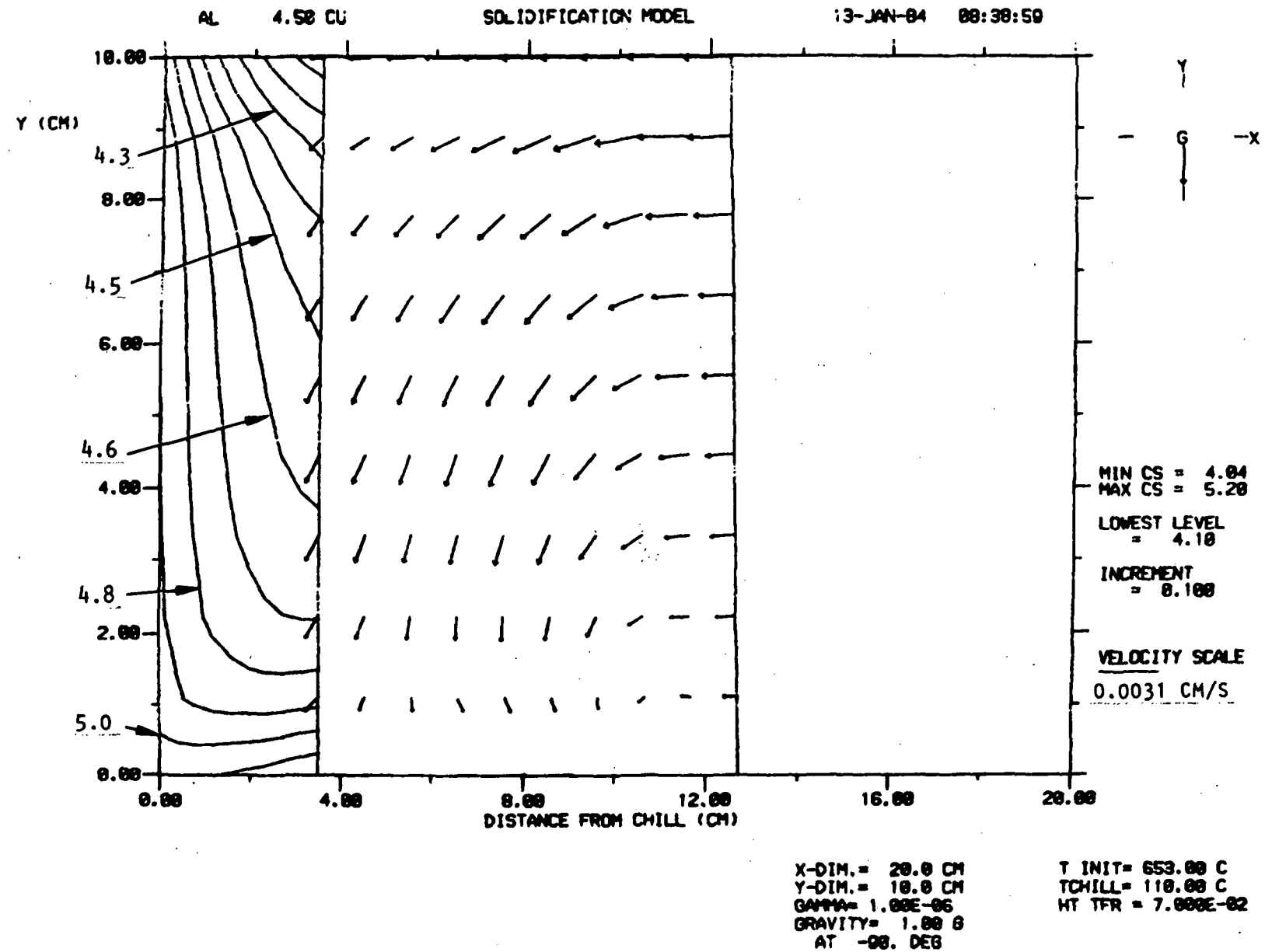

Figure 3.15. Final Local Average Composition and Interdendritic Fluid Velocity at t = 400 Seconds

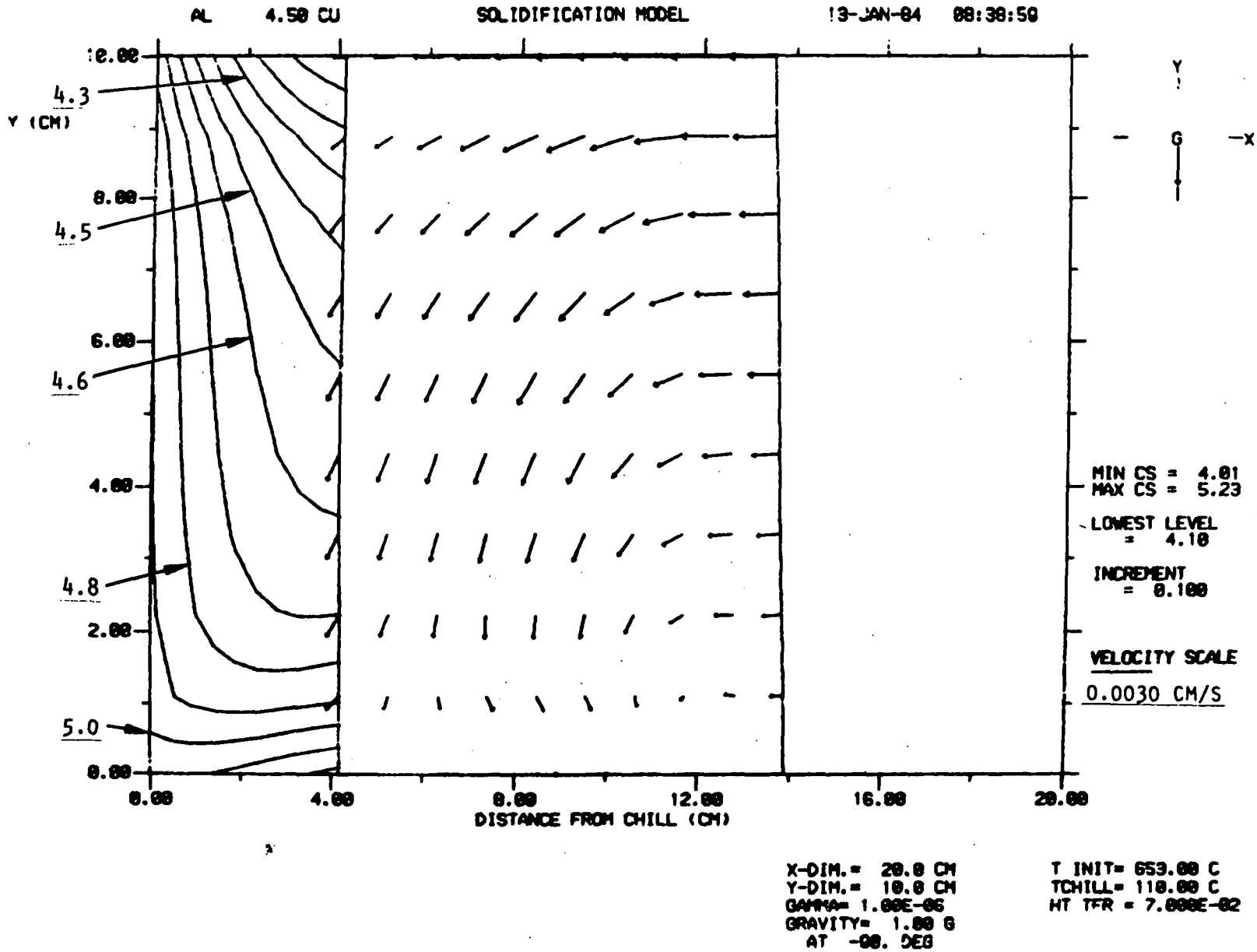

Figure 3.16. Final Local Average Composition and Interdendritic Fluid Velocity at t = 451 Seconds

As the completely solid-region grows out from the chill the final local average composition is indicated by contour lines at intervals of 0.1 wt. pct. Cu. The last figure in the sequence, Fig. 3.16, is at 451 seconds from the beginning of solidification when the calculation stopped due to failure to obtain convergence in the Newton-Raphson iteration procedure. Preliminary testing indicated the problem was caused by an inadequate approximation in the calculation of the total-mass conservation elements of the Jacobian matrix. The maximum reverse flow velocity along the lower boundary is about an order of magnitude slower than the isotherm velocity, so freckling is not considered to be a contributing factor. An alternative procedure with an uncoupled solution of the total-mass conservation equation is partially complete at the time of this writing.

SECTION 4
FLOW IN THE BULK LIQUID

In Section 3 and in the previous reports on this research (9-11), the convection in the "bulk liquid" is ignored. The region containing the bulk liquid is shown in Fig. 3.1. By ignoring the convection in the bulk liquid, the pressure along the liquidus isotherm can be specified as

$$p = p_0 + \rho_L g\,(Y-y) \tag{4.1}$$

where p_0 is the pressure at $x = X$ and $y = Y$ (the ambient pressure) and ρ_L is the density of the bulk liquid. A more rigorous solution to the solidification of an alloy would include a coupling of the convective field in the bulk liquid to the convective field in the S/L zone. An approach is described in this section.

4.1 Physical Description

In the bulk liquid region shown in Fig. 3.1 there is two-dimensional convection because the temperature in this region is not uniform. If the thermal properties of the liquid are constant, then the continuity, momentum and energy equations (25) are

$$\nabla \cdot \vec{v} = 0, \tag{4.1.1}$$

$$\frac{\partial \vec{v}}{\partial t} + \vec{v} \cdot \nabla \vec{v} = -\frac{1}{\rho_L} \nabla p + \nu \nabla^2 \vec{v}\,, \tag{4.1.2}$$

and

$$\frac{\partial T}{\partial t} + \vec{v} \cdot \nabla T = \alpha \nabla^2 T \tag{4.1.3}$$

in which ν is the kinematic viscosity and α is the thermal diffusivity.

The assumption of constant properties can be relaxed when solutions to Eqs. (4.1.1)-(4.1.3) are obtained numerically. The properties can be assigned according to the local temperatures; the approximation neglects nonlinear terms which are very small.

To treat natural convection, Wilkes and Churchill (26) define a pressure which the deviation from the initial static pressure; a similar definition (but not exactly equal) of pressure is used herein for the pressure in the bulk liquid. It is

$$\hat{p} = p - \left[p_0 + \rho_{Li} g\ (Y-y)\right] \tag{4.1.4}$$

with ρ_{Li} as the initial density of the liquid and p_0 as the ambient pressure. With $\hat{p}$ defined according to Eq. (4.1.4) it is consistent with the modified pressure in Eq. (4.5.1) of Maples and Poirier (9).

The volume expansion coefficient, defined as

$$\beta = -\frac{1}{\rho_L}\frac{\partial \rho_L}{\partial T},$$

is approximated as

$$\beta \simeq \frac{1}{\rho_L}\left(\frac{\rho_{Li} - \rho_L}{T - T_i}\right). \tag{4.1.5}$$

Then with $g_x = 0$, $g_y = -g$ and by using Eqs. (4.1.4) and (4.1.5), the components of Eq. (4.1.2) can be written as

$$\frac{\partial v_x}{\partial t} + v_x\frac{\partial v_x}{\partial x} + v_y\frac{\partial v_x}{\partial y} = -\frac{1}{\rho}\frac{\partial \hat{p}}{\partial x} + \nu\left(\frac{\partial^2 v_x}{\partial x^2} + \frac{\partial^2 v_x}{\partial y^2}\right) \tag{4.1.6}$$

and

$$\frac{\partial v_y}{\partial t} + v_x\frac{\partial v_y}{\partial x} + v_y\frac{\partial v_y}{\partial y} = -\frac{1}{\rho}\frac{\partial \hat{p}}{\partial y} + \beta g\ (T-T_i) + \nu\left(\frac{\partial^2 v_y}{\partial x^2} + \frac{\partial^2 v_y}{\partial y^2}\right) \tag{4.1.7}$$

Ridder (8) considered the natural convection in the bulk liquid above the S/L region of an ingot solidifiying upwards. In his analysis, he assumed $\partial p/\partial x = 0$, $\partial p/\partial y = 0$ and $\bar{\rho}_L/\rho_L \simeq 1$ where $\bar{\rho}$ is the density of the liquid at a reference temperature $\bar{T}$. Then

$$\rho_L = \bar{\rho}_L\ \left[1-\beta\ (T-\bar{T})\right]$$

and the components of Eq. (4.1.2) become

$$\frac{\partial v_x}{\partial t} + v_x \frac{\partial v_x}{\partial x} + v_y \frac{\partial v_x}{\partial y} = \nu \left(\frac{\partial^2 v_x}{\partial x^2} + \frac{\partial^2 v_x}{\partial y^2} \right) \tag{4.1.8}$$

and

$$\frac{\partial v_y}{\partial t} + v_x \frac{\partial v_y}{\partial x} + v_y \frac{\partial v_y}{\partial y} = \beta g \, (T - \bar{T}) + \nu \left(\frac{\partial^2 v_y}{\partial x^2} + \frac{\partial^2 v_y}{\partial y^2} \right). \tag{4.1.9}$$

Note that Eqs. (4.1.8) and (4.1.9) contain no terms for pressure (or modified $\hat{p}$) which implies that $(\partial \hat{p}/\partial x) = (\partial \hat{p}/\partial y) = 0$. This is only absolutely valid if, in fact, there is no convection. As the convection increases, Eqs. (4.1.8) and (4.1.4) become less valid; consequently, Eqs. (4.1.6) and (4.1.7) should be more appropriate to use over a wider range of convective conditions.

4.2 Numerical Methods

Previous investigators (26, 27-31) of natural convection in enclosures have all recast their approximations to Eq. (4.1.2) into a vorticity equation before seeking a numerical solution. Following the method of Wilkes and Churchill (26) the following procedure is employed:

1. Eqs. (4.1.6) and (4.1.7) are differentiated with respect to y and x, respectively;
2. the results are subtracted; and
3. Eq. (4.1.1) is applied.

This gives an equation in which pressure does not appear.

$$\frac{\partial}{\partial t} \left(\frac{\partial v_x}{\partial y} - \frac{\partial v_y}{\partial x} \right) + v_x \frac{\partial^2 v_x}{\partial x \partial y} + v_y \frac{\partial^2 v_x}{\partial y^2} - v_x \frac{\partial^2 v_y}{\partial x^2} - v_y \frac{\partial^2 v_y}{\partial x \partial y} =$$

$$-\beta g \frac{\partial T}{\partial x} + \nu \left(\frac{\partial}{\partial y} \nabla^2 v_x - \frac{\partial}{\partial x} \nabla^2 v_y \right) \tag{4.2.1}$$

Next, the vorticity is defined as

$$\xi = \frac{\partial v_y}{\partial x} - \frac{\partial v_x}{\partial y} \tag{4.2.2}$$

and the stream function as

$$v_x = \frac{\partial \psi}{\partial y} \; ; \; v_y = - \frac{\partial \psi}{\partial x} \; . \tag{4.2.3}$$

Moreover, ξ and ψ are related by (26, 32)

$$\xi = - \left[\frac{\partial^2 \psi}{\partial x^2} + \frac{\partial^2 \psi}{\partial y^2} \right] = -\nabla^2 \psi \; . \tag{4.2.4}$$

By making use of Eq. (4.2.1), Eq. (4.2.2) becomes:

$$\frac{\partial \xi}{\partial t} + v_x \frac{\partial \xi}{\partial x} + v_y \frac{\partial \xi}{\partial y} = \beta g \frac{\partial T}{\partial x} + \nu \nabla^2 \xi \tag{4.2.5}$$

The governing equations are now summarized:

Vorticity Equation - Eq. (4.2.5),
Energy Equation - Eq. (4.1.3),
Stream Function Equation - (Eq. (4.2.4), and
Velocity Equation - Eq. (4.2.3).

The relationships presented herein can be used to calculate the velocity and temperature fields in the bulk liquid provided the natural convection is laminar. Since the system, comprising a S/L region encroaching upon a diminishing bulk liquid as depicted in Fig. 3.1, has not been studied for the limit of laminar stability, we examine related systems to predict the applicability of the governing equations.

To determine whether flow is laminar or turbulent, the Rayleigh number is calculated. The form of the Rayleigh number and its critical value depend on the type of thermal boundary condition at x = 0 (see Fig. 3.1) and the characteristic dimension selected for the system; several examples follow.

Uniform Heat Flux at x = 0

For a vertical surface of length Y, the Rayleigh number is defined by

$$Ra = \frac{g \beta Y^4 q}{k_T \nu \alpha} \tag{4.2.6}$$

in which q is the uniform heat flux applied at x = 0. If Ra < 10^{12}, the convection is laminar (31).

In a rectangular enclosure of width X and length Y oriented with its length along the vertical, the Rayleigh number is defined as

$$Ra = \frac{g\beta X^4 q}{k_T \nu\alpha} \quad . \tag{4.2.7}$$

If Ra < 3 x 10^6, the convection is laminar (31).

Uniform Temperature at x = 0

For a vertical surface of length Y, the Rayleigh number is

$$Ra = \frac{g\beta Y^3 \Delta T}{\nu\alpha} \quad . \tag{4.2.8}$$

Here ΔT is the temperature difference between the vertical surface and the liquid. If Ra < 10^9, the convection is laminar (32).

In a rectangular enclosure of width X and length Y oriented with its length along the vertical, the Rayleigh number is

$$Ra = \frac{g\beta X^4 \Delta T}{\nu\alpha} \quad . \tag{4.2.9}$$

If Ra < 10^7 flow is laminar (33).

In order to estimate an appropriate value of q to be used in Eqs. (4.2.6) and (4.2.7), data on the cooling rate of Sn -15% Pb alloy before solidification were used. The alloy was contained in a mold of the dimensions Y = 6.35 cm and X = 2.7 cm. Using the maximum cooling rate observed, 0.25 ^{o}C/S, the heat flux into the chill surface (i.e., q at x = 0) was computed by means of a simple energy applied to the alloy melt.

A value of 25^{o}C was used for ΔT in Eqs. (4.2.8) and (4.2.9). Since the temperature gradients within a convecting bulk liquid of a solidifying alloy

are small for the type of system considered, herein, the value of 25°C is quite conservative.

The results of the calculations are summarized in Table 1.

Table 1

Summary of Calculations for Rayleigh Numbers

Equation for Rayleigh Number	Critical Rayleigh Number	Calculated Rayleigh Numbers	
		Sn-15% Pb	Al-4% Cu
Eq. (4.2.6)	10^{12}	10^{6}	5×10^{4}
Eq. (4.2.7)	3×10^{6}	3×10^{4}	2×10^{3}
Eq. (4.2.8)	10^{9}	10^{6}	2×10^{5}
Eq. (4.2.9)	10^{7}	8×10^{4}	10^{4}

In all cases, the Rayleigh numbers are well below those at which laminar convection would become unstable. Although the exact system is not duplicated, these numbers show that the assumption of laminar flow in the bulk liquid is valid.

After solidification proceeds, the characteristic dimension (in the cases of Eqs. (4.2.7) and (4.2.9)) would decrease; also, q and/or ΔT would decrease. All of these factors reduce the Rayleigh numbers to values less than the calculated values shown in Table 1.

Although Table 1 clearly shows that the convection in the bulk liquid is expected to be laminar, numerical calculations of previous workers indicate unstable results when the Grashof number exceeds a critical value. The unstable results have been attributed to the errors and approximations involved in the numerical schemes and should not be confused with a critical value of the Rayeligh number which indicates the laminar to turbulent transition. The Grashof number is defined as

$$Gr = \frac{g\beta\rho_L^2 L\Delta T}{\mu^2} \qquad (4.2.10)$$

in which L is a characteristic dimension of the system (e.g., Y and X in Eqs. 4.2.6-4.2.9). The Rayleigh number and the Grashof number are related by

$$Ra = Gr \cdot Pr \qquad (4.2.11)$$

in which Pr is the Prandtl number (ν/α) of the bulk liquid. For the alloys considered in Table 1, the Prandtl numbers are approximately 0.02-0.03 so the Grashof numbers would be in the range $5x10^2$ to $2x10^4$ for the Sn-15% Pb alloy and $3x10^2$ to $7x10^3$ for the Al-4% Cu alloy.

Previous workers (8,26-30) who have sought numerical solutions to natural convection in enclosures report that difficulties in obtaining stable solutions occur at Grashof numbers which exceed the range (10^2 - 10^4) to be encountered in this work. For example, in 1966 Wilkes and Churchill (26) report that they obtained numerical instabilities whenever the Grashof number exceeded $2x10^5$. More recently (1981) Desai and Kim (28) reported stable numerical results for Grashof numbers in excess of 10^6, and in a study of the bulk liquid convection above a solid-liquid region in a solidifying ingot, Ridder (8) achieved stable solutions for Grashof numbers up to approximately $2x10^6$.

SECTION 5
OPERATING GUIDE

5.1 Running the Interactive Models

In 1982 the models were converted to operate in interactive mode on a Digital Equipment Corporation VAX 11/780. The following discussion pertains to operating the model on a VAX, although only the starting procedure is system-dependent. The log-in procedure may vary from installation to installation and so is not described here.

5.1.1 Starting the Solidification Model

After logging in, the user initiates execution of the program by entering one command: MPS 3. The model identification page will appear on the screen shortly after this command is entered.

5.1.2 Input Phase

For each case, the program passes through three phases of operation. The first is the input phase during which the user defines the case to be run by specifying the case title, the alloy and the values of the model parameters. At each step the program clearly specifies the type of information it requires. The code is able to trap and recover from input errors, thus avoiding fatal FORTRAN I/O errors which would necessitate restarting the program. The input parameters are defined in a later section. Each time execution is initiated the built-in default case will appear in the model. If any parameter is changed during the input phase, the new value will remain in effect through subsequent cases in the same session or until it is changed again. Copies of the input phase displays are shown in the examples section.

As described in reference 11, the input phase is controlled at a higher level so that the operator need only review the parameter classifications that are to be changed. After the case title is input the following selection appears on the screen:

```
ENTER  P  TO PROCEED TO CALCULATION
       1  TO CHANGE ALLOY
       2  TO REVIEW ALLOY DATA
       3  TO REVIEW OR CHANGE SOLIDIFICATION PROCESS PARAMETERS
       4  TO REVIEW OR CHANGE PERMEABILITY MODEL PARAMETERS
       5  TO REVIEW OR CHANGE NUMERICAL METHODS CONTROL PARAMETERS
```

If the operator selects one of 1 - 5 then the input phase proceeds directly to that classification. Upon exiting the classification, control returns to the higher level selection shown above. Thus the operator can move through the input at will. When he is satisfied with all input values, the "P" selection initiates the calculation. Some operational notes for each step of the input phase follow.

- The case title is simply typed in; if none is desired, push RETURN.
- For binary alloys, the solvent and solute are entered as (uppercase) chemical symbols with no leading or embedded blanks. The program then checks the alloy data base, and if the data for the requested alloy is found, it is displayed on the screen. If the alloy is not in the data base, an error message and a list of alloys in the data base are displayed, and the user is allowed to select another alloy.
- The remaining parameters are grouped under several broad classificiations; each group is a separate display page in the input phase. When a parameter is changed, the display is refreshed with the new value. The user can change any, all, or none of the parameters in a group before returning to the higher control level.

5.1.3 Calculation Phase

When the operator enters "P" during the input phase, the model begins the second stage of operation, the calculation phase. During this phase, the program determines the numerical solution to the equations describing the model subject to the conditions defined by the input parameters.

After the input phase is complete, the model takes one step away from the chill and then prints the message shown below.

```
ENTER T TO DISPLAY TABULAR DATA,
      G TO DISPLAY GRAPHS,
      C TO CONTINUE THIS CASE,
      Q TO TERMINATE RUN, OR
      N TO PROCEED TO NEXT CASE.
```

This choice of action is given to the user at each checkpoint. Entering a G or a T will cause the program to go to the output phase in which the user can select specific graphical or tabular output from the calculation up to that point. When the user leaves the output phase, the selection shown above is again presented. The user can switch freely between tabular and graphical output or he can continue the calculation, start a new case or terminate execution. If the continue (C) option is selected, the program will display the following:

```
TIME SINCE BEGINNING OF SOLIDIFICAITON = 1.0000    SEC.

ENTER THE TIME OF THE NEXT CHECK POINT.
```

The checkpoint procedure puts the user in control of the progress of the calculation. The stopping places specified by the user as checkpoints allow him to inspect the progress of the calculation or display the current state of the S/L zone at any point in the solidification process. The stopping point is specified as a time simply by tying in the stopping time in seconds. For example,

10.

The program then resumes the calculation and displays

```
CONTINUING CALCULATION.....
```

5.1.4 Output Phase

The three levels of operation during the output phase are illustrated in Figure 5.1. At the highest level the user can choose to display graphical output, to display tabular output, to terminate execution of the program, or to terminate the case by proceeding to the next case.

- At the graphical output level the user is given a choice of functions to plot and types of plot to use as shown in example 5.4. Immediately after entry of the plot type, the plot will be generated on the screen*. When the cursor remains motionless at the upper left corner of the screen, the plot is complete. To leave the plot display and return to plot selection mode, enter a P.

- At the tabular output level the display commences immediately after user selection of a function. Each time the screen in filled, the program waits for the user to enter a P before proceeding to the next display page or to the function selection page. On a typical 20 X 20 mesh a scalar function such as g_L requires only one page while a vector function such as velocity requires three pages.

- Note that it is possible to switch freely between graphical and tabular output at the highest control level and to repeat the plot of a given function with a variety of scaling choices.

- After entering a Q to terminate execution or an N to proceed to the next case, the user can return to output mode only by re-running the case.

5.2 Input Parameters

5.2.1 Process Parameters

The parameters in this group describe the conditions under which the casting is made including the mold geometry, the thermal conditions, and the strength and direction of the gravitational force.

Parameter Description	(Symbol)	Default	Limits
Mold half width	X	8 cm	$X > 0$
Mold height	Y	10 cm	$Y > 0$
Initial temperature of melt	--	668 °C/sec	greater than T_{LO}
Temperature of chill	T_{chill}	30 °C/sec	$T_{chill} < T_E$
Heat transfer coefficient at chill	(h)	0.1608	$h > 0$
Gravitational force	(g)	1 G	$g > 0$
Angle of g with x-axis	-	-90.	-360 to 360

* In some cases, the user is given the opportunity to override the computed scale with an input scale.

5.2.2 Permeability Model Parameters

The permeability model is identical to that defined in Ref. 11.

Parameters	Symbol	Default	Limits
Reference value of gamma	γ_o	6×10^{-7} cm^2	$\gamma_o > 0$
Reference arm spacing	d_o	1. micron	$d_o > 0$
Dendrite-arm spacing exponent	q_γ	0.	$q_\gamma > 0$
Solidification-time coefficient	a_d	1.	$a_d > 0$
Solidification-time exponent	q_d	0.	$q_d > 0.$
y location of grain boundary	-	0. cm	0. to L
γ multiplier at grain boundary	-	1.	0

The default values were selected so that $\gamma = \gamma_o$ with no grain boundary.

5.2.3 Numerical Methods Control Parameters

In the vast majority of cases the parameters in this group should not be changed from their default values, however operator control of these parameters could be useful in trouble-shooting.

Parameter Description	(Symbol)	Default	Limits
Number of x-mesh points in the liquid	(N_L)	10	$10 \leq N_L \leq 40$
Number of x-mesh points in the mush	(N_M)	10	$10 \leq N_M \leq 40$
Number of x-mesh points in the solid	(N_S)	10	$10 \leq N_S \leq 40$
Number of y-mesh points	(N_Y)	10	$3 \leq N_Y \leq 20$
Time step size	(Δt)	1.	$\Delta t > 0.$

5.3 Alloy Data Base Structure

The alloy data base contains alloy properties used by the solidification model. The use of a separate data base automatically accessed by the model frees the user from inputting relatively static alloy data with each change in mold contents, yet it allows complete flexibility in the range of alloys which can be processed. The phase diagram, density data and viscosity data for each

alloy are included as well as a reference block allowing notation of data sources. The data base is in card image format and can be modified by using any system text editor.

CARD	FORMAT	CONTENTS
1	20A4	Data base identifier
2	A4,6X,A4,6X,2E10.3	Solvent, solute, minimum C_L, maximum C_L
3	20A4	5 cards for notation of data sources
4	"	
5	"	
6	"	
7	"	
8	4E10.3	dC_L/dT, k, C_E, T_E
9	4E10.3	$d\rho_L/dC_L$, ρ_S, ρ_{LE}, ρ_{SE}
10	E10.3	μ
11	7E10.3	$H_L^*, H_S^*, H_E^*, C_{PL}, C_{PSL}, C_{PSE}, C_{PE}$
12	4E10.3	a_L, b_L, a_E, b_E
13	5E10.3	$a_{SLO}, b_{SLO}, T_{HILO}, a_{SHI}, b_{SHI}$

Cards 2 through 13 are repeated for each alloy system.

```
ALLOY DATA BASE  -  DATA BASE FOR MODEL 3  -  CONTAINS THERMAL DATA

SOURCE OF INFORMATION FOR  AL  -CU        0.000E+00 TO  3.300E+01 WT. PCT. CU
   PHASE DIAGRAM - M.C. FLEMINGS AND G. NEREO, MET TRANS, VOL 239, 1967, P 1449.
   DENSITIES,    - R.MEHRABIAN, M.KEANE AND M.C.FLEMINGS, TRANS TMS-AIME,
    VISCOSITY      VOL 1, 1970, P 1209.
   THERMAL DATA  - D.R. POIRIER, UNIVERSITY OF ARIZONA


PHASE DIAGRAM
   TEMPERATURE-COMPOSITION SLOPE                -2.000E-01 PCT SOLUTE / DEG C
   EQUILIBRIUM PARTITION RATIO                   1.720E-01
   EUTECTIC COMPOSITION                          3.300E+01 PCT SOLUTE
   EUTECTIC TEMPERATURE                          5.480E+02 DEG C


DENSITIES
   COMPOSITION-DENSITY SLOPE                     2.670E-02 (GM/CM**3) / PCT SOLUTE
   SOLID DENSITY                                 2.620E+00 GM/CM**3
   LIQUID EUTECTIC DENSITY                       3.220E+00 GM/CM**3
   SOLID EUTECTIC DENSITY                        3.400E+00 GM/CM**3


VISCOSITY                                        3.000E-02 GM/(CM*SEC)


REFERENCE ENTHALPY LEVELS (J/GM)
   HSTL=  3.916E+02   HSTS=  0.000E+00   HSTE= -2.778E+02

SPECIFIC HEATS ( J/(GM*DEG C) )
   CPLL=  1.050E+00   CPSL=  1.310E+00   CPSE=  1.033E+00   CPEE=  8.370E-01

THERMAL CONDUCTIVITY (J/(CM*S*DEG C))  COEFFICIENTS
   AKL=     4.180E-04   BKL=     8.670E-01
   AKE=     0.000E+00   BKE=     0.000E+00
   AKSLO= -2.000E-03   BKSLO=  7.000E-01
   THILO=  3.270E+02
   AKSHI=  5.270E-04   BKSHI=  1.206E+00


ENTER P TO PROCEED
```

```
AL     4.5Ø CU              SOLIDIFICATION MODEL              12-JAN-84   12:07:ØØ


SOLIDIFICATION PROCESS PARAMETERS
 1     MOLD (HALF) WIDTH  (X DIRECTION)        2.ØØØE+Ø1     (CM)
 2     MOLD HEIGHT        (Y DIRECTION)        1.ØØØE+Ø1     (CM)
 3     INITIAL TEMPERATURE OF MELT             6.53ØE+Ø2     (DEG C)
 4     TEMPERATURE OF CHILL                    1.1ØØE+Ø2     (DEG C)
 5     HEAT TRANSFER COEFFICIENT AT CHILL      7.ØØØE-Ø2     (J/CM**2/SEC/DEG C)
 6     GRAVITATIONAL FORCE                     1.ØØØE+ØØ     (G)
 7     ANGLE WITH X-AXIS    (Ø= +X, -ØØ= -Y)  -9.ØØØE+Ø1     (DEG)


ENTER ITEM NUMBER TO CHANGE, OR
      P              TO PROCEED.


AL     4.5Ø CU              SOLIDIFICATION MODEL              12-JAN-84   12:07:ØØ


PERMEABILITY MODEL PARAMETERS
 1     GAMMAØ                                  1.ØØØE-Ø6     (CM**2)
 2     DØ                                      1.ØØØE+ØØ     (MICRONS)
 3     DENDRITE-ARM-SPACING EXPONENT (QG)      Ø.ØØØE+ØØ
 4     SOLIDIFICATION-TIME COEFFICIENT (AD)    1.ØØØE+ØØ     (FOR D IN MICRONS)
 5     SOLIDIFICATION-TIME EXPONENT (QD)       Ø.ØØØE+ØØ


ENTER ITEM NUMBER TO CHANGE, OR
      P              TO PROCEED.


AL     4.5Ø CU              SOLIDIFICATION MODEL              12-JAN-84   12:15:56


NUMERICAL METHODS CONTROL PARAMETERS
 1     NUMBER OF X-MESH POINTS IN THE LIQUID       1Ø
 2     NUMBER OF X-MESH POINTS IN THE MUSH         1Ø
 3     NUMBER OF X-MESH POINTS IN THE SOLID        1Ø
 4     NUMBER OF Y-MESH POINTS                     1Ø
 5     TIME STEP SIZE                          1.ØØØE+ØØ     (SEC)


ENTER ITEM NUMBER TO CHANGE, OR
      P              TO PROCEED.
```

```
AL     4.50 CU            SOLIDIFICATION MODEL            12-JAN-84   12:07:00


ENTER  P  TO PROCEED TO CALCULATION
       1  TO CHANGE ALLOY
       2  TO REVIEW ALLOY DATA
       3  TO REVIEW OR CHANGE SOLIDIFICATION PROCESS PARAMETERS
       4  TO REVIEW OR CHANGE PERMEABILITY MODEL PARAMETERS
       5  TO REVIEW OR CHANGE NUMERICAL METHODS CONTROL PARAMETERS
P

TIME SINCE BEGINNING OF SOLIDIFICATION =  1.00000     SEC.


ENTER  T TO DISPLAY TABULAR DATA,
       O TO MODIFY PRINTED OUTPUT CONTROL
       G TO DISPLAY GRAPHS,
       C TO CONTINUE THIS CASE,
       Q TO TERMINATE RUN, OR
       N TO PROCEED TO NEXT CASE.
C

TIME SINCE BEGINNING OF SOLIDIFICATION =  1.00000     SEC.

ENTER THE TIME OF THE NEXT CHECKPOINT
400.

AL     4.50 CU            SOLIDIFICATION MODEL            11-JAN-84   00:00:21


CONTOUR, VECTOR PLOTS
   1   ISOTHERMS
   2   FINAL COMPOSITION OF SOLID, VELOCITY OF LIQUID
   3   CONTOURS OF FRACTION EUTECTIC, FRACTION LIQUID

PROFILE PLOTS
   4   TEMPERATURE
   5   FINAL LOCAL AVERAGE COMPOSITION
   6   VOLUME FRACTION EUTECTIC
   7   VOLUME FRACTION LIQUID
   8   PRESSURE: P-P0
   9   PRESSURE - METALLOSTATIC PRESSURE
  10   TIME  VS  LIQUIDUS LOCATION
  11   TIME  VS  EUTECTIC LOCATION


ENTER ITEM NUMBER OF PLOT OR P TO PROCEED
1

ENTER THE NUMBER OF CONTOUR INTERVALS TO INSERT BETWEEN THE LIQUIDUS AND EUTECTIC TEMPERATURES
10
```

5.4 Sample Case (Cont.)

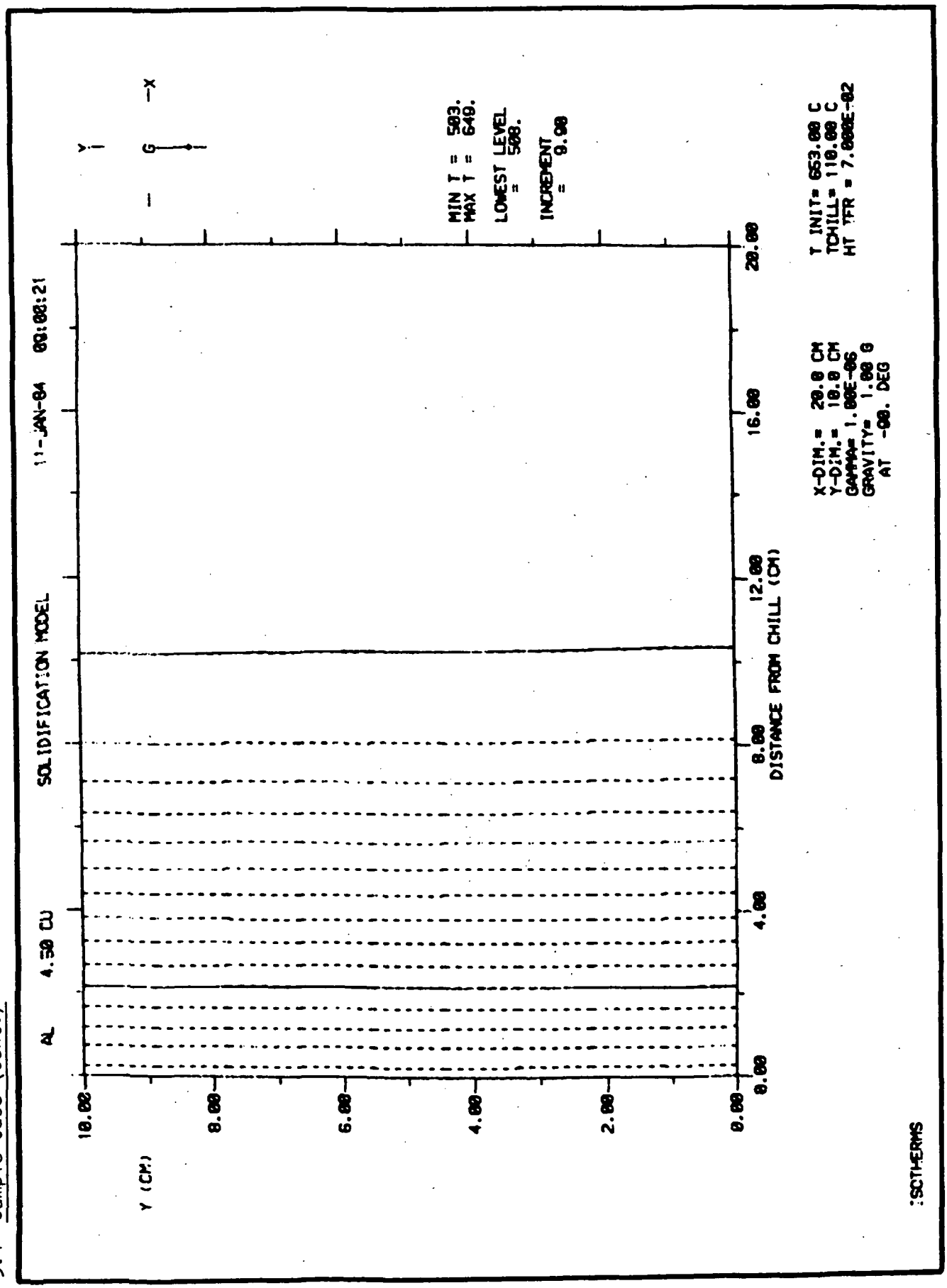

```
AL     4.50 CU            SOLIDIFICATION MODEL            11-JAN-84   09:00:21


CONTOUR, VECTOR PLOTS
   1   ISOTHERMS
   2   FINAL COMPOSITION OF SOLID, VELOCITY OF LIQUID
   3   CONTOURS OF FRACTION EUTECTIC, FRACTION LIQUID

PROFILE PLOTS
   4   TEMPERATURE
   5   FINAL LOCAL AVERAGE COMPOSITION
   6   VOLUME FRACTION EUTECTIC
   7   VOLUME FRACTION LIQUID
   8   PRESSURE: P-P0
   9   PRESSURE - METALLOSTATIC PRESSURE
  10   TIME  VS  LIQUIDUS LOCATION
  11   TIME  VS  EUTECTIC LOCATION


ENTER ITEM NUMBER OF PLOT OR P TO PROCEED
2


MINIMUM COMPOSITION OF FINAL SOLID = 4.187E+00
MAXIMUM COMPOSITION OF FINAL SOLID = 5.134E+00

ENTER THE INTERVAL BETWEEN LEVELS
.1


COMPUTED MAXIMUM VELOCITY = 3.293E-03
ENTER SCALE VELOCITY, OR
     P TO PROCEED WITH SCALE= MAXIMUM VELOCITY
P
```

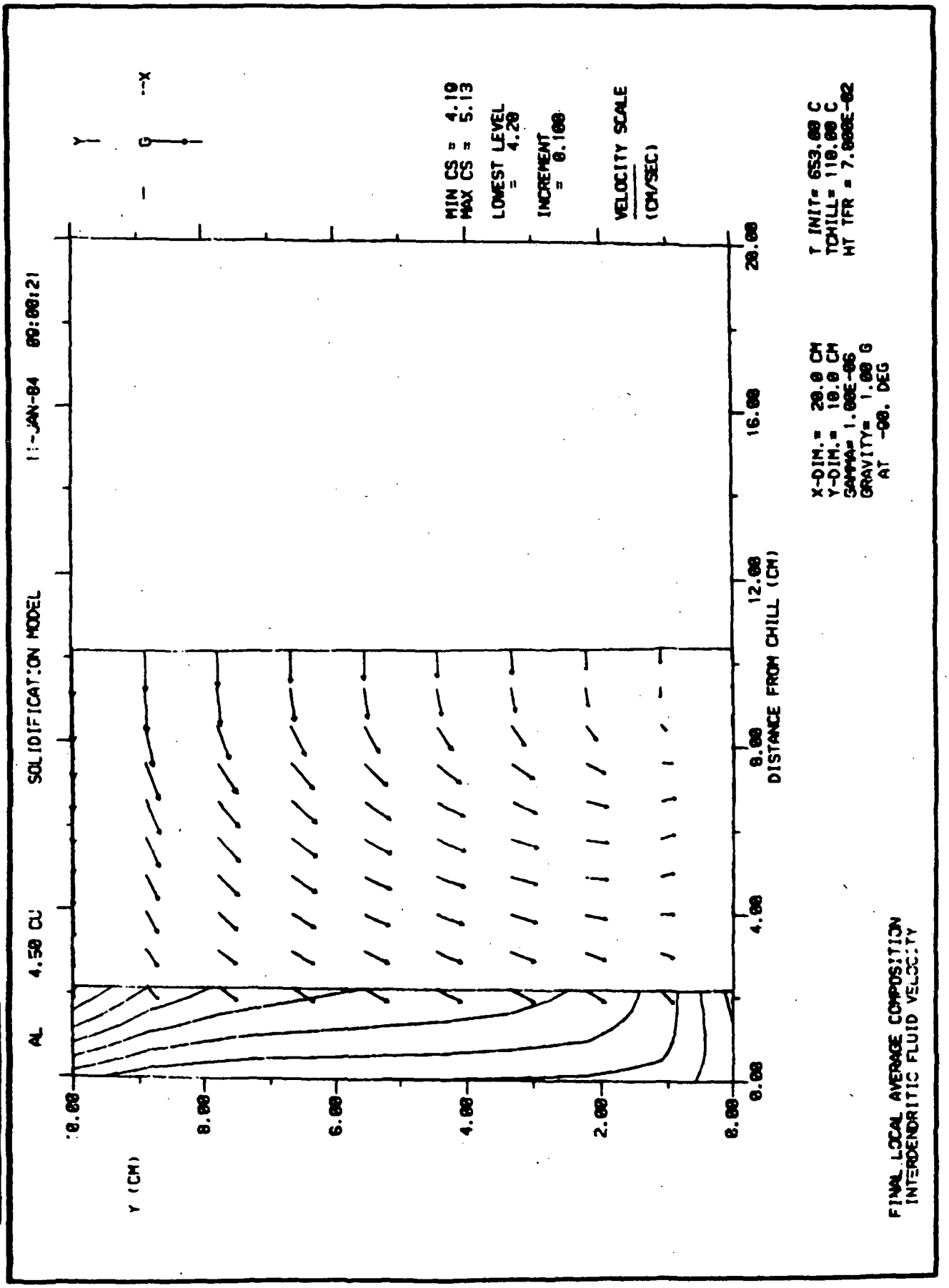
AL 4.50 CU SOLIDIFICATION MODEL 11-JAN-84 00:00:21
MIN CS = 4.10
MAX CS = 5.13
LOWEST LEVEL = 4.20
INCREMENT = 0.100
VELOCITY SCALE (CM/SEC)
Y
G
X
Y (CM)
DISTANCE FROM CHILL (CM)
X-DIM.= 20.0 CM
Y-DIM.= 10.0 CM
GAMMA= 1.00E-05
GRAVITY= 1.00 G
AT -90. DEG
T INIT= 653.00 C
TCHILL= 110.00 C
HT TFR = 7.000E-02
FINAL LOCAL AVERAGE COMPOSITION
INTERDENDRITIC FLUID VELOCITY

```
AL     4.50 CU              SOLIDIFICATION MODEL              11-JAN-84   00:00:21


CONTOUR, VECTOR PLOTS
   1    ISOTHERMS
   2    FINAL COMPOSITION OF SOLID, VELOCITY OF LIQUID
   3    CONTOURS OF FRACTION EUTECTIC, FRACTION LIQUID

PROFILE PLOTS
   4    TEMPERATURE
   5    FINAL LOCAL AVERAGE COMPOSITION
   6    VOLUME FRACTION EUTECTIC
   7    VOLUME FRACTION LIQUID
   8    PRESSURE: P-P0
   9    PRESSURE - METALLOSTATIC PRESSURE
  10    TIME  VS  LIQUIDUS LOCATION
  11    TIME  VS  EUTECTIC LOCATION


ENTER ITEM NUMBER OF PLOT OR P TO PROCEED
3


MINIMUM VOLUME FRACTION EUTECTIC = 6.373E-02
MAXIMUM VOLUME FRACTION EUTECTIC = 8.666E-02

ENTER THE BASE LEVEL
.06

ENTER THE INTERVAL BETWEEN LEVELS
.005


MINIMUM VOLUME FRACTION LIQUID = 6.373E-02
MAXIMUM VOLUME FRACTION LIQUID = 1.000E+00

ENTER THE BASE LEVEL
1.

ENTER THE INTERVAL BETWEEN LEVELS
.1
```

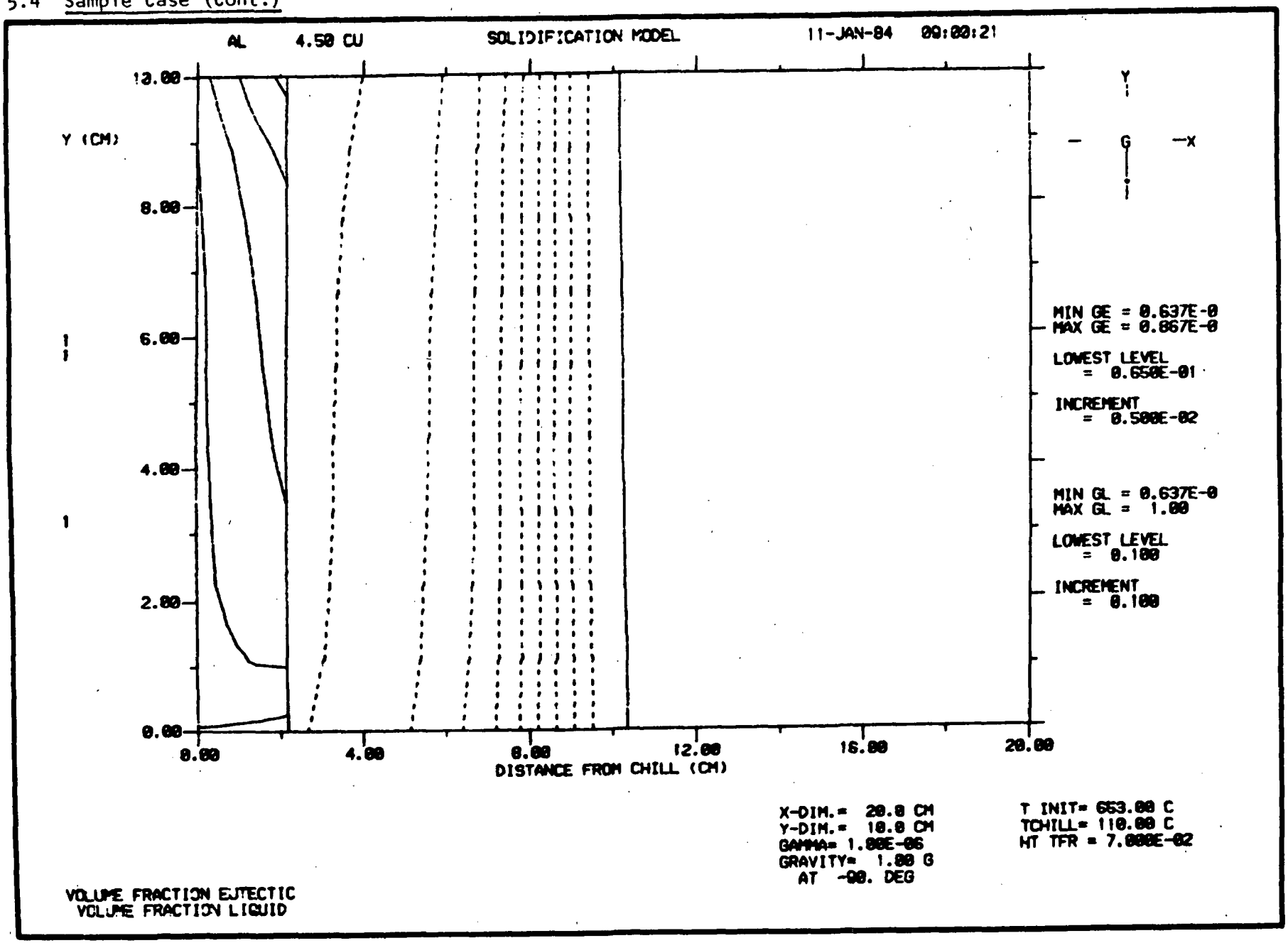
AL 4.50 CU
SOLIDIFICATION MODEL
11-JAN-84 09:00:21
Y (CM)
12.00
8.00
6.00
4.00
2.00
0.00
0.00
4.00
8.00
12.00
16.00
20.00
DISTANCE FROM CHILL (CM)
Y
G
X
MIN GE = 0.637E-0
MAX GE = 0.867E-0
LOWEST LEVEL
= 0.650E-01
INCREMENT
= 0.500E-02
MIN GL = 0.637E-0
MAX GL = 1.00
LOWEST LEVEL
= 0.100
INCREMENT
= 0.100
X-DIM.= 20.0 CM
Y-DIM.= 10.0 CM
GAMMA= 1.00E-06
GRAVITY= 1.00 G
AT -90. DEG
T INIT= 653.00 C
TCHILL= 110.00 C
HT TFR = 7.000E-02
VOLUME FRACTION EUTECTIC
VOLUME FRACTION LIQUID

```
                                                                    10.
AL     4.50 CU              SOLIDIFICATION MODEL          ENTER ITEM NUMBER OF PROFILE OR P TO PROCEED


CONTOUR, VECTOR PLOTS
   1   ISOTHERMS
   2   FINAL COMPOSITION OF SOLID, VELOCITY OF LIQUID
   3   CONTOURS OF FRACTION EUTECTIC, FRACTION LIQUID

PROFILE PLOTS
   4   TEMPERATURE
   5   FINAL LOCAL AVERAGE COMPOSITION
   6   VOLUME FRACTION EUTECTIC
   7   VOLUME FRACTION LIQUID
   8   PRESSURE: P-P0
   9   PRESSURE - METALLOSTATIC PRESSURE
  10   TIME  VS  LIQUIDUS LOCATION
  11   TIME  VS  EUTECTIC LOCATION


ENTER ITEM NUMBER OF PLOT OR P TO PROCEED
4


ENTER X OR Y FOR X-PROFILES OR Y-PROFILES
X


MINIMUM FUNCTION VALUE =  502.505
MAXIMUM FUNCTION VALUE =  649.159

AUTOMATIC SCALING YIELDS PLOT RANGE:   500.000 TO 650.000 WITH REMOTE EXPONENT    0
OVER  8 MAJOR TIC INTERVALS

ENTER P TO PROCEED WITH AUTOMATIC SCALING, OR
      LOWER BOUND OF PLOT INTERVAL.
360.

ENTER UPPER BOUND OF PLOT INTERVAL
660.

ENTER REMOTE EXPONENT
0

ENTER NUMBER OF MAJOR TIC INTERVALS
3
ENTER Y VALUE OF PROFILE OR P TO PROCEED
0.
ENTER Y VALUE OF PROFILE OR P TO PROCEED
5.
ENTER Y VALUE OF PROFILE OR P TO PROCEED
```

5.4 Sample Case (Final)

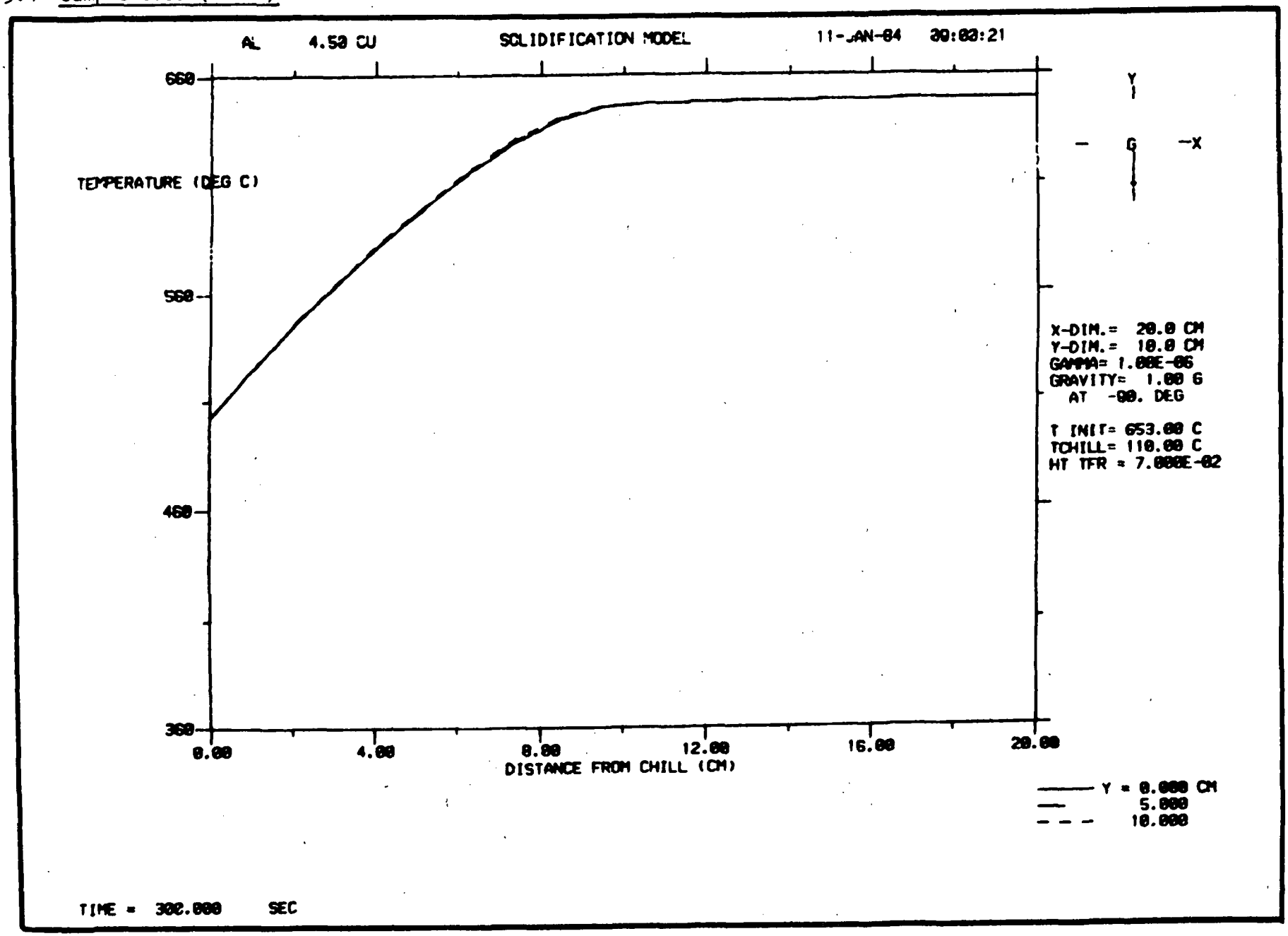

SECTION 6
SOFTWARE DOCUMENTATION

6.1 Flow Diagrams

6.1.1 Global Flow Diagram

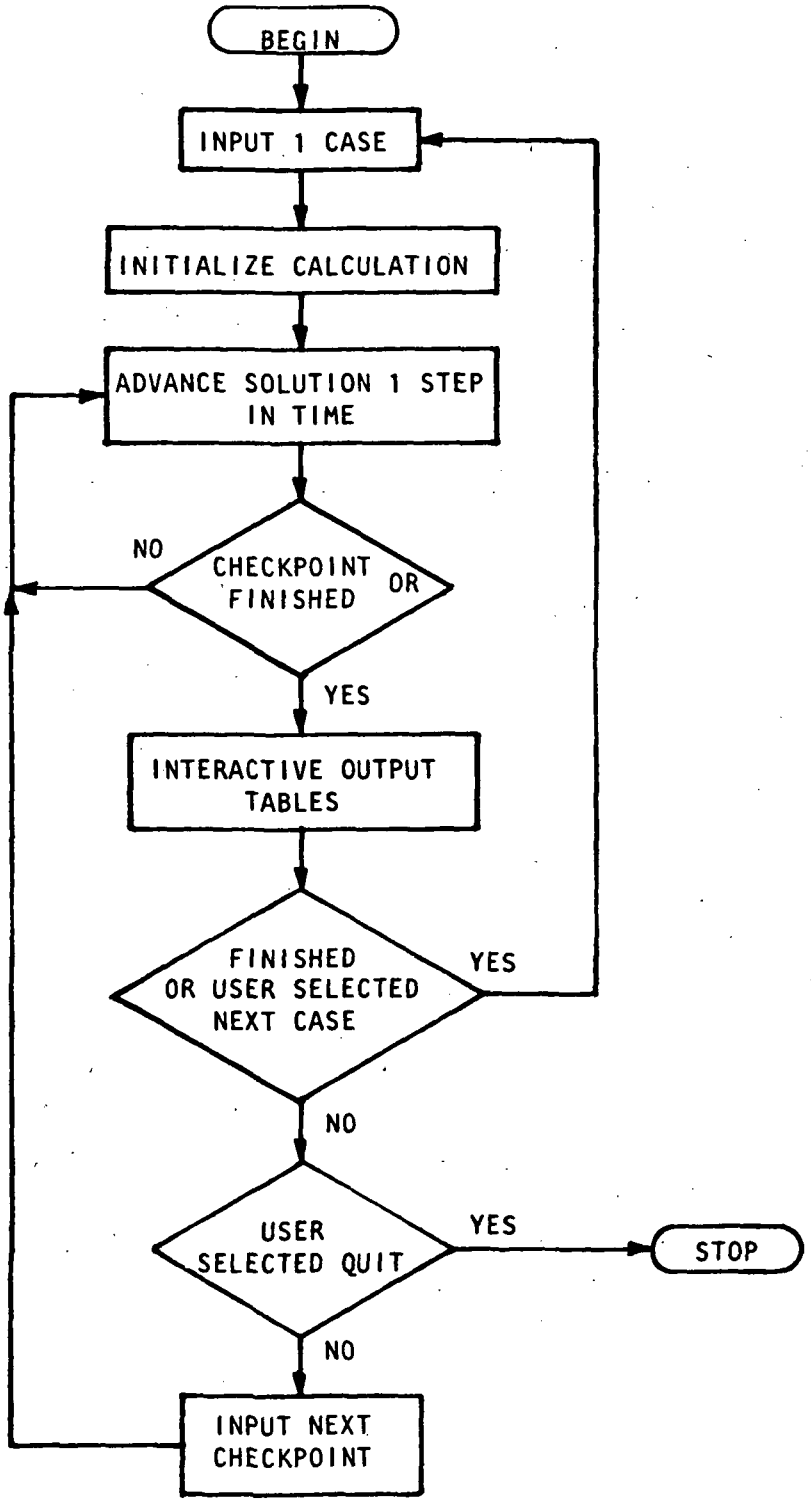

6.1.2 Calculation Section

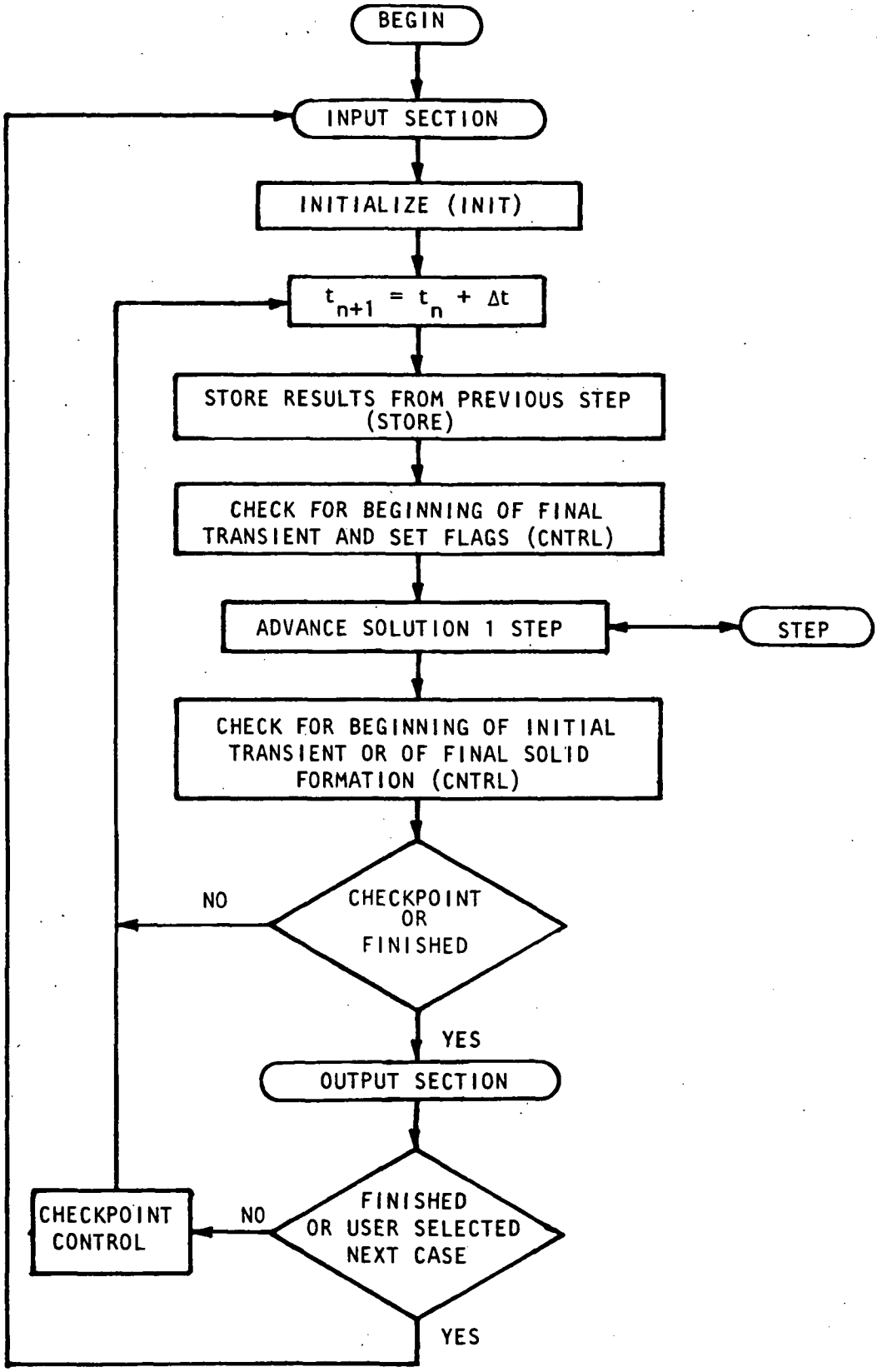

6.1.2 Calculation Section (Continued)

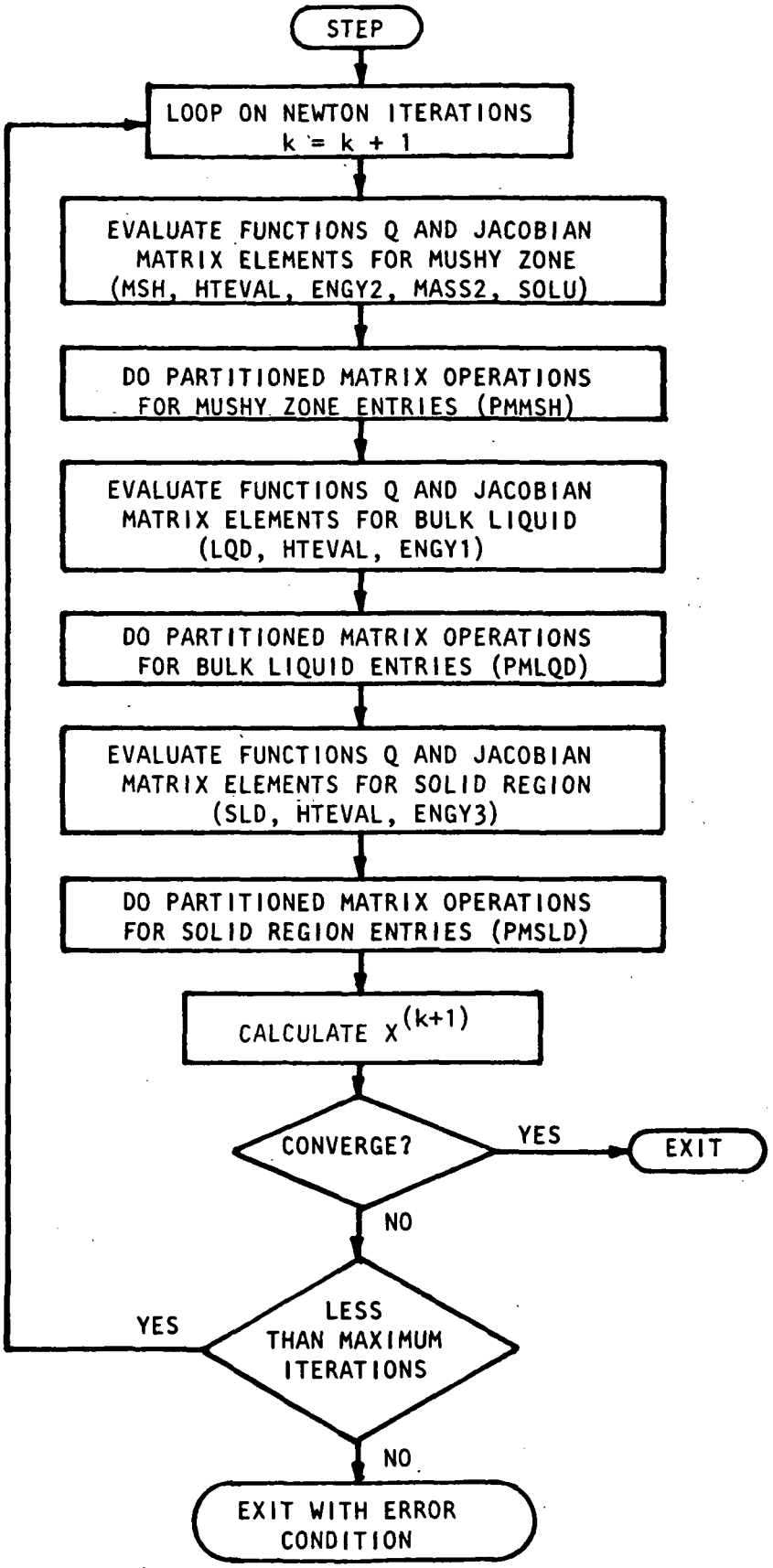

6.1.3 Input Section

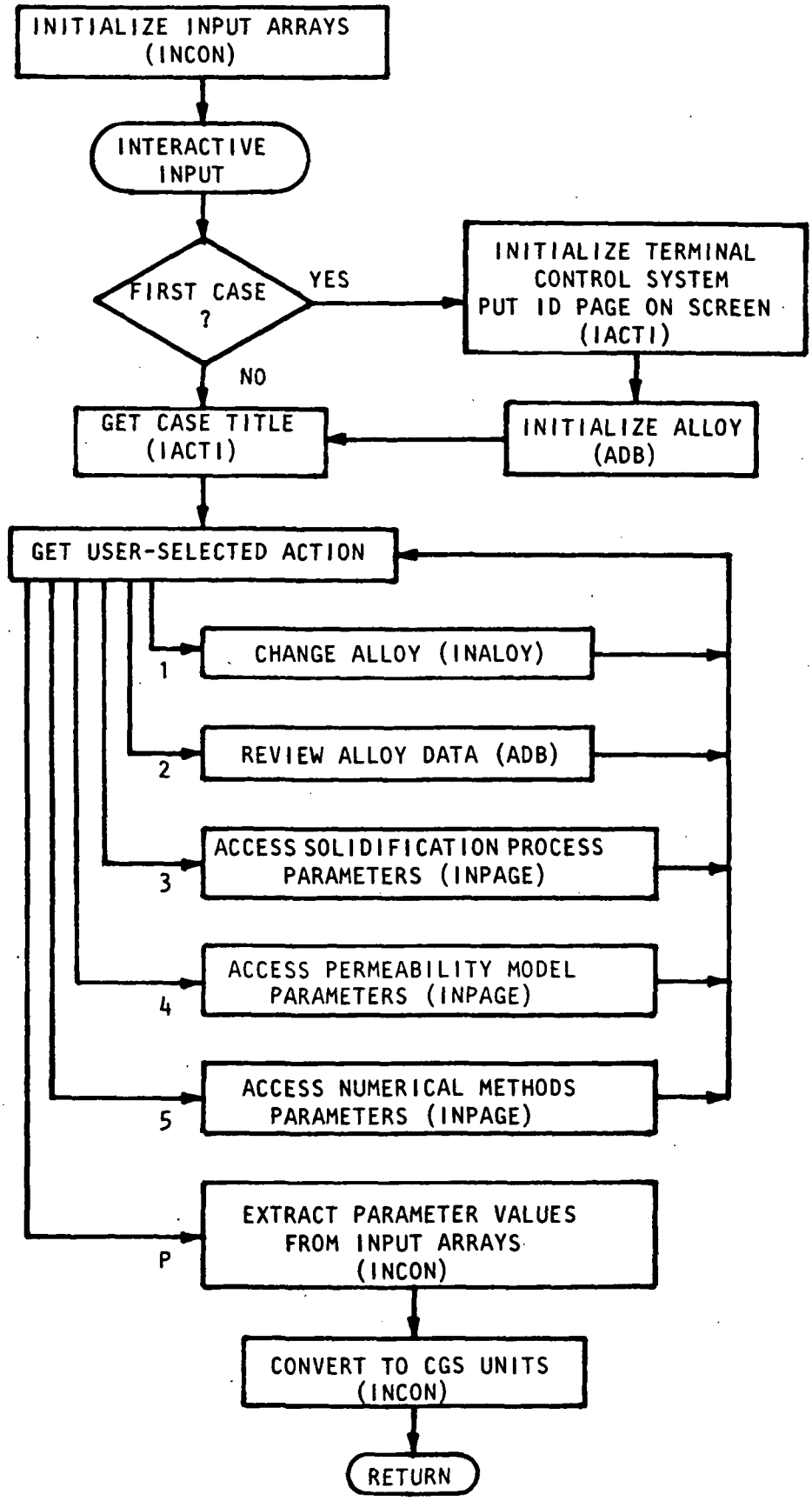

6.1.4 Output Section

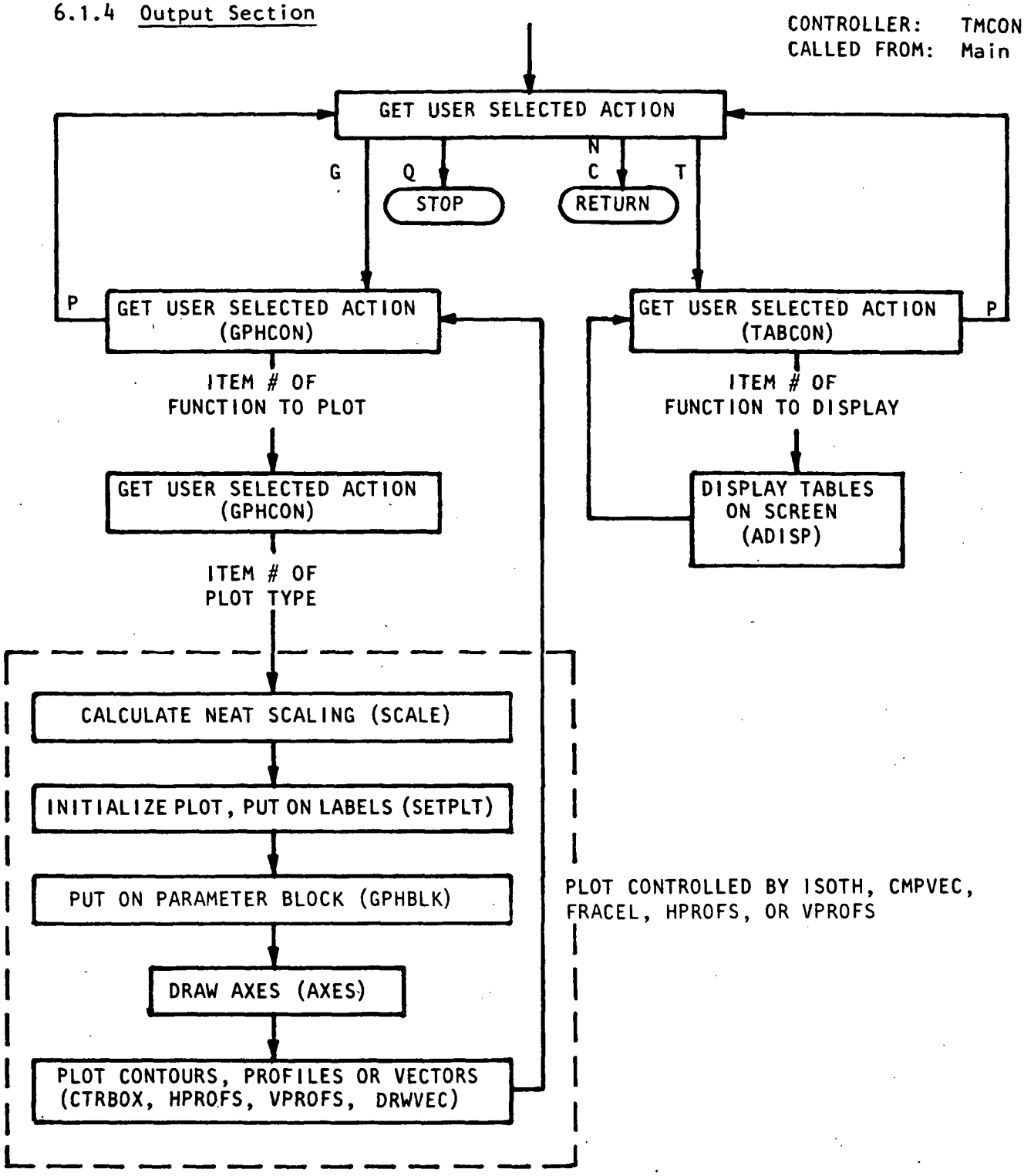

6.2 Alphabetical Listing of Subroutines

The list below contains only the modules that were written specifically for the solidification model. VAX/VUS routines and Tektronix routines called by the model are listed in Ref. 11.

Calculation Modules

NAME	FUNCTION
CNTRL	Tests for and controls change of calculation phase, for example from all-liquid conditions to the beginning of the initial transient.
CROSS	Locates the position where temperature has an input value.
DNSTY	Calculates functions associated with density.
ENGY1,2,3	Evaluate Q and the Jacobian elements for the energy equation in the liquid, mush and solid, respectively.
FINSLD	Calculates macrosegregation in the final solid.
GLINT	Interpolates volume fraction liquid.
HOFT	Evaluates enthalpy as a function of temperature.
HTEVAL	Evaluates Q and the Jacobian elements for the enthalpy-temperature relationship in each of the three regions.
INIT	Initialization routine.
LQD	Controls the calculation of information for the bulk liquid region during the Newton-Raphson iterations.
MASS2	Evaluates Q and the Jacobian elements for the total-mass conservation equation in the mushy zone.
MSH	Controls the calculation of information for the mushy zone during the Newton-Raphson iterations.
PENTA	Solves penta-diagonal matrix equations.
PERM	Evaluates the permeability function.
PMLQD	Performs partitioned matrix calculations for elements from the bulk liquid region.
PMMSH	Performs partitioned matrix calculations for elements from the mush zone.
PMSLD	Performs partitioned matrix calculations for elements from the solid region.
SLD	Controls the calculation of information for the solid region during the Newton-Raphson iterations.

SOLU	Evaluates Q and the Jacobian elements for the solute-mass conservation equation in the mushy zone.
SPLIT	Called by CNTRL to separate the temperature array into arrays over two regions.
STEP	Controls the Newton-Raphson iterations.
STORE	Stores arrays from the previous time prior to taking another time step.
STRECH	Interpolates a static array over a growing region.
THCOND	Evaluates the thermal conductivity.
TRI2,3	Solve tridiagonal matrix equations.
VLCTY	Evaluates the velocity from Darcy's Law.
XYCALC	Calculates some of the coefficients of the coordinate transformation.

Input Modules

All input modules are the same as those listed in Ref. 11.

Graphics Modules

NAME	FUNCTION
AXES	Draws and labels axes.
CMPVEC	Plots composition contours and velocity vectors.
CTRBOX	Controls contouring within a grid cell.
CTRDRW	Draws contour lines.
DRWVEC	Draws arrows for vector plots.
FRACEL	Plots contours of fraction eutectic and fraction liquid.
GPBLK	Puts parameter block on plots.
GPHCON	Controls graphical output.
GPHG	Puts gravity vector on plots.
HPROFS	Draws horizontal profiles.
INGOT	Sets up axes and labels for plots on whole ingot.
ISOTH	Plots isotherms throughout casting.
PRFINT	Interpolates profiles between grid points.
SCALE	Calculates neat scaling.
SETPLT	Initializes plot.
VPROFS	Draws vertical profiles.
XLABEL	Sets up label for horizontal axis.

6.3 Key Program Symbols

PROGRAM SYMBOL	COMMON BLOCK	DEFINITION
ACS	/AUX/	$\overline{C}_S$
CL	/AUX/	C_L
DX11,DX12,DX13	/MESH/	$\Delta\xi_L, \Delta\xi_M, \Delta\mu_S$
DYE	/MESH/	$\Delta\eta$
GL	/STATE/	g_L
GE	/AUX/	g_E
H1,H2,H3	/STATE/	$\overline{\rho H}$ in the liquid, mush, solid
NI1,NI2,NI3	/MESH/	N_L, N_M, N_S
NJ	/MESH/	N_Y
P2	/STATE/	p
RL2	/AUX/	p_L
T1,T2,T3	/STATE/	T in the liquid, mush, solid
V	/AUX/	v
XC	/MESH/	x
XI1,XI2,XI3	/MESH/	ξ_L, ξ_M, ξ_S
XL,XE	/MESH/	x_L and x_E at each j
YE	/MESH/	η
YY	/CTSFM/	Y

SECTION 7

REFERENCES

1. R. Mehrabian, M. Keane, and M. C. Flemings: Met. Trans., 1970, vol. 1, pp. 1209-1220.

2. S. Kou, D. R. Poirier, and M. C. Flemings: In Proceedings of the Electric Furnace Conference, Iron and Steel Society of AIME, December, 1977, pp. 221-228.

3. M. C. Flemings and G. E. Nereo: Trans. TMS-AIME, 1967, vol. 239, pp. 1449-1461.

4. M. C. Flemings, R. Mehrabian, and G. E. Nereo: Trans. TMS-AIME, 1968, vol. 242, pp. 41-49.

5. M. C. Flemings and G. E. Nereo: Trans. TMS-AIME, 1968, vol. 242, pp. 50-55.

6. R. Mehrabian, M. Keane, and M. C. Flemings: Met Trans., 1970, vol. 1, pp. 3238-3241.

7. T. Fujii, D. R. Poirier, and M. C. Flemings: Met. Trans. B, 1979, vol. 10B, pp. 331-339.

8. S. D. Ridder: Ph.D. Thesis, University of Illinois at Urbana-Champaign, 1980.

9. A. L. Maples and D. R. Poirier: Report No. 80HV007, Vol. I-III, General Electric Company, Huntsville, Alabama, 1980.

10. D. R. Poirier and A. L. Maples: Report No. 81HV001, Vol. I and II, General Electric Company, Huntsville, Alabama, 1981.

11. A. L. Maples and D. R. Poirier: Report No. 83HV004, General Electric Company, Huntsville, Alabama, 1983.

12. A. L. Maples, "A Technique for Solving Moving Boundary Problems." In the Proceedings of the 1983 Engineering Foundation Conference on the Modeling of Casting and Welding Processes, J. A. Dantzig and J. T. Berry (eds.), to be published.

13. J. Crank, "How to Deal with Moving Boundaries in Thermal Problems." In Numerical Methods in Heat Transfer, R. Lewis, K. Morgan, and O. Zienkiewiez (eds.), John Wiley & Sons Ltd., 1981, pp 177-200.

14. J. Crank and R. S. Gupta, J. Inst. Math. Applic., 1972, vol. 10, pp. 19-23.

15. J. Crank and R. S. Gupta, J. Inst. Math. Applic., 1972, vol. 10, pp. 296-304.

16. N. Shamsundar and E. M. Sparrow: J. Heat Transfer, Trans. ASME(C), 1975, vol. 97, pp. 333-340.

17. N. Shamsundar and E. M. Sparrow: J. Heat Transfer, Trans. ASME(C), 1976, vol. 98, pp. 550-557.

18. S. D. Murray and F. Landis: J. Heat Transfer, Trans. ASME(C), 1959, vol. 81, pp. 106-112.

19. R. Bonnerot and P. Jamet: Inst. J. Num. Meth. Engineering, 1974, vol. 8, pp. 811-820.

20. J. F. Thompson, F. C. Thames, and C. W. Mastin: J. Computational Physics, 1974, vol. 15, pp. 299-319.

21. H. Viviand: LaRecherche Aerospatiale, 1974, pp. 65-68.

22. G. Dahlquist, A. Bjorck, and N. Anderson: Numerical Methods, pp. 249-251, Prentice-Hall, New Jersey, 1974.

23. J. Szekely and N. J. Themelis: Rate Phenomena in Process Metallurgy, p. 331, Wiley-Interscience, New York, 1971.

24. V. Koump, R. H. Tien, and T. F. Perzak: Trans. TMS-AIME, 1968, vol. 242, pp. 1569-1574.

25. G. H. Geiger and D. R. Poirier: Transport Phenomena in Metallurgy, pp. 54, 55, 235, Addison-Wesley, Reading, MA, 1973.

26. J. O. Wilkes and S. W. Churchill, A.I.Ch.E.J., 1966, vol. 12 (No. 1), pp. 161-166.

27. P. V. Desai and F. Rastegar: "Convection in Mold Cavities" in H. D. Brody and D. Apelian (eds.), Modeling of Casting and Welding Processes, TMS of AIME, Warrendale, PA, 1981, pp. 351-359.

28. P. V. Desai and C. Kim: "On Convection in Liquid Metal Molds." In Proceedings of Second International Conference on Numerical Methods in Thermal Problems, Venice, Italy, July, 1981.

29. S. D. Ridder, S. Kou and R. Mehrabian: Metall. Trans. B, 1981, vol. 12B, pp. 435-447.

30. J. Szekely and A. S. Jassal: Metall. Trans. B, 1978, vol. 9B, pp. 389-398.

31. B. V. Karlekar and R. M. Desmond: Engineering Heat Transfer, p. 451, West Publishing, St. Paul, 1977.

32. G. H. Geiger and D. R. Poirier: Transport Phenomena in Metallurgy, p. 254, Addison-Wesley, Reading, MA, 1973.

33. J. P. Holman, Heat Transfer, 3rd ed., p. 222, McGraw-Hill, New York, 1972.

34. Y. S. Toulonkian, R. W. Powell, C. Y. Ho, and P. G. Klemens: Thermophysical Properties of Matter, vol. 1, p. 9, IFI/Plenum, New York, 1970.

35. L. F. Mondolfo: Aluminum Alloys: Structure and Properties, p. 60, Buttersworth, London, 1976.

36. M. M. Mebed, H. A. Khalek, and M. Abd Elnaiem in T. N. Veziroglu (ed): Proceedings of Condensed Papers, Sixteenth Southeastern Seminar on Thermal Sciences, April 1982, Miami, Florida, pp. 13-15.

37. Y. S. Toulonkian, R. W. Powell, C. Y. Ho, and P. G. Klemens: ibid., p. 408.

38. Y. S. Toulonkian, R. W. Powell, C. Y. Ho, and P. G. Klemens: ibid., p. 191.

39. Y. S. Toulonkian, R. W. Powell, C. Y. Ho, and P. G. Klemens: ibid., p. 652.

40. R. A. Swalin: Thermodynamics of Solids, pp. 60-61, John Wiley, New York, 1962.

41. D. R. Gaskell: Introduction to Metallurgical Thermodynamics, pp. 124, 130, 151, McGraw-Hill, New York, 1973.

42. C. E. Sims (ed.): Electric Furnace Steelmaking - vol. II Theory and Fundamentals, p. 45, Interscience, New York, 1963.

43. R. Hultgren, P. D. Desai, D. T. Hawkins, M. Gleiser and K. K. Kelley: Selected Values of the Thermodynamic Properties of Binary Alloys, pp. 151-155, 1266-1268, American Society for Metals, Metals Park, Ohio, 1973.

44. R. Hultgren, P. D. Desai, D. T. Hawkins, M. Gleiser, K. K. Kelley and D. D. Wagman: Selected Values of the Thermodynamic Properties of the Elements, pp. 382, 482, American Society for Metals, Metals park, Ohio, 1973.

APPENDIX A

THERMAL PROPERTIES

A.1 Enthalpy - Temperature Coefficients

The following values were derived from Appendix B which is an analysis of the enthalpies of the solidifying alloys.

	Al-4.5 wt. pct. Cu	Sn-15 wt. pct. Pb
C_{PL}	1.059 (J/gm°C)	0.237 (J/gm°C)
C_{PSL}	1.310 (J/gm°C)	0.250 (J/gm°C)
C_{PSE}	1.033 (J/gm°C)	0.243 (J/gm°C)
C_{PE}	0.837 (J/gm°C)	0.161 (J/gm°C)
H_L^*	391.6 (J/gm)	54.27 (J/gm)
H_S^*	0. (J/gm)	0. (J/gm)
H_E^*	-277.8 (J/gm)	-13.39 (J/gm)

A.2 Thermal Conductivity of Al-4.5 wt. pct. Cu (Ref. 34-36)

(All thermal conductivities are in units J/cm.s.°C.)

solid: $k_{TS} = -2.09\times10^{-3} (T-T_E) + 0.709$ if $27^\circ C < T < 327^\circ C$

$k_{TS} = 5.27\times10^{-4} (T-T_E) + 1.286$ if $327^\circ C < T < 645^\circ C$

liquid: $k_{TL} = 4.18\times10^{-4} (T-T_E) + 0.867$ if $T > 548^\circ C$

S/L: $k_T = g_S k_{TS} + g_L k_{TL}$

A.3 Thermal Conductivity of Sn-15 wt. pct. Cu (Ref. 37-39)

(All thermal conductivities are in units J/cm.s.°C.)

solid: $k_T = g_S k_{TS} + g_E k_{TE}$

with $k_{TS} = -4.39\times10^{-4} (T-T_E) + 0.599$ if $T < 183^\circ C$

$k_{TE} = -2.30\times10^{-4} (T-T_E) + 0.426$ if $T < 183^\circ C$

liquid: $k_{TL} = 2.07\times10^{-4} (T-T_E) + 0.292$ if $T > 183^\circ C$

S/L: $k_T = g_S k_{TS} + g_L k_{TL}$

with $k_{TS} = -2.70\times10^{-4} (T-T_E) + 0.609$ if $T > 183^\circ C$

APPENDIX B
SOLIDIFICATION ENTHALPIES AND THE EFFECT OF MACROSEGREGATION ON ENTHALPY

B.1 The Enthalpy of the Primary Solid

The solid is assumed to be a regular solution so that its enthalpy (for a binary system) is given by

$$H_S = \frac{X_1 H^0_{1S} + X_2 H^0_{2S} + \alpha_S X_1 X_2}{X_1 M_1 + X_2 M_2} \qquad (B.1)$$

where

H_S = enthalpy of the solid (cal/g)

X_1, X_2 = mole fractions of components 1 and 2, respectively,

H^0_{1S}, H^0_{2S} = molar enthalpies of the pure components as solids (cal/mole),

α_S = constant which depends upon the heat of mixing for the solid (cal/mole), and

M_1, M_2 = atomic weights (g/mole).

The enthalpies of the pure components, themselves, are temperature dependent and are given by

$$H^0_i = a_i (T-298) + \frac{b_i}{2} (T^2-298^2) + c_i (298^{-1}-T^{-1}) \qquad (B.2)$$

where

T = absolute temperature (K),

and a_i, b_i and c_i are empirical constants for the specific heats. In particular, the specific heats are expressed as

$$C_{pi} = a_i + b_i T + c_i T^{-2} \qquad (B.3)$$

with C_{pi} in (cal/mole-K).

B.2 The Enthalpy of the Liquid

The liquid is assumed to be a regular solution so that its enthalpy (for a binary) is given by

$$H_L = \frac{X_1 H^0_{1L} + X_2 H^0_{2L} + \alpha_L X_1 X_2}{X_1 M_1 + X_2 M_2} \qquad (B.4)$$

H_L = enthalpy of the liquid (cal/g),

H^0_{1L}, H^0_{2L} = molar enthalpies of the pure components as liquids (cal/mole),

α_L = constant which depends upon the heat of mixing for the liquid (cal/mole).

The enthalpies of the pure components are

$$H^0_{iL} = (H^0_{im} + \Delta H_{fi}) + \int_{T_{mi}}^{T} (d_i + e_i T + g_i T^{-2})\, dT \qquad (B.5)$$

where

H^0_{im} = enthalpy of the pure solid i at its melting point (cal/mole)

ΔH_{fi} = heat of solidification for pure i (cal/mole),

T_{mi} = melting point of pure i (K), and

d_i, e_i, g_i = empirical constants for the molar specific heat of liquid i.

The integration of Eq. (B.5) yields:

$$H^0_{iL} = (H^0_{im} + \Delta H_{fi}) + e_i(T - T_{mi}) + \frac{f_i}{2}(T^2 - T^2_{mi}) + g_i(T^{-1}_{mi} - T^{-1}) \qquad (B.6)$$

B.3 The Enthalpy of the Eutectic Constituent

Two types of eutectic are considered:

1. the eutectic is a mixture of a terminal and an intermetallic phase (e.g., in Al-Cu alloys), and
2. the eutectic is a mixture of two terminal phases (e.g., in Sn-Pb alloys).

When the eutectic comprises a terminal phase and an intermetallic phase, the enthalpy is

$$H_E = f_I H_I + (1-f_I)H_\alpha \qquad (B.7)$$

in which

H_E = enthalpy of the eutectic mixture (cal/g),
H_I = enthalpy of the intermetallic phase (cal/g),
H_α = enthalpy of the terminal phase (cal/g), and
f_I = weight fraction of the intermetallic phase in the eutectic mixture.

The enthalpy of the intermetallic phase is estimated by using the Neumann-Kopp rule (40) for its molar specific heat; accordingly

$$C_{PI} = mC_{P1} + nC_{P2} \qquad (B.8)$$

and

$$H_I = \frac{\Delta H_{298} + mH_1^0 + nH_2^0}{mM_1 + nM_2} . \qquad (B.9)$$

Here,

C_{PI} = molar heat capacity of the intermetallic phase (cal/mole-K),
m,n = stoichiometric proportions in the intermetallic phase, and
ΔH_{298} = heat of formation at 298K.

In Eq. (B.7), H_α is evaluated by Eq. (B.1) in which $H_S = H_\alpha$ and X_2 is the mole fraction of solute in the terminal phase within the eutectic mixture.

When the eutectic comprises two terminal phases, the enthalpy is

$$H_E = f_\alpha H_\alpha + f_\beta H_\beta \qquad (B.10)$$

where

H_α, H_β = enthalpies of the terminal solid solutions making up the eutectic (cal/g), and

f_α, f_β = weight fractions of the terminal solid solutions in the eutectic.

In Eq. (B.10), H_α and H_β are evaluated by Eq. (B.1) with X_2 as the mole fraction of solute in the respective terminal phases in the eutectic mixture.

B.4 The Enthalpy of Solidifying Alloys

The enthalpy of the alloy when it comprises both solid and liquid is

$$\bar{\rho}H = (1-g_L)\rho_S H_S + g_L \rho_L H_L \quad T_E \leq T < T_{LO} \qquad (B.11)$$

where,

ρ_S, ρ_L = mass densities of the solid and liquid phases (g/cm^3) respectively,

g_L = volume fraction of liquid, and

$\bar{\rho}$ = $(1-g_L)\rho_S + g_L\rho_L$, the average density of the solid-liquid mixture.

Upon complete solidification, the alloy comprises the eutectic constituent and the primary solid. Thus

$$\bar{\rho}H = (1-g_E)\rho_S H_S + g_E \rho_{SE} H_E \quad T \leq T_E \qquad (B.12)$$

where,

g_E = volume fraction of eutectic, and

ρ_{SE} = mass density of the eutectic (g/cm^3).

In this case, the average density of the solidified alloy is

$$\bar{\rho} = (1-g_E)\rho_S + g_E \rho_{SE} \cdot \qquad (B.13)$$

B.5 The Enthalpy of Al-4.5% Cu and Sn-15% Pb Alloys During Solidification

During solidification and after solidification as the alloy cools, the enthalpy is a function of the local macrosegregation since enthalpy depends upon the relative amounts of the constituents and the composition of the constituents. Specifically, in the S/L temperature range the relative amounts of the phases as well as the local average composition of the dendritic solid depends upon the specific solidification conditions at that locale, and after solidification the local fraction of the eutectic constituent (and hence local average composition) can vary substantially from point-to-point within the costing or ingot. Hence, enthalpy can not be treated as a function of temperature only. Preliminary calculations showed, indeed, that enthalpy depends strongly on the degree of macrosegregation at a specific location. However, the effect of the average composition of the primary dendritic solid on the enthalpy of the solid can be neglected. This simplifies the computation of enthalpy in that the enthalpy of the alloy comprises the enthalpies of the *liquid, solid and eutectic constituents in accordance with their relative* amounts regardless of the average composition of the primary solid.

Figure B1 shows the results of computing enthalpy for the three constituents in Al-4.5% Cu alloy. For the liquid-phase there is a unique curve since the composition of the liquid above and below the liquidus temperature is a function only of temperature regardless of the local flow and macrosegregation conditions. For the primary solid two curves are shown, each corresponding to a very different macrosegregation condition. In one case, the net flow of interdendritic liquid has been strongly positive resulting a volume fraction of eutectic of 0.20 and an average composition after solidification of 9.5% Cu. In the other case, the volume fraction of eutectic is 0.066 and the average composition is only 3.45% Cu. Thus, one curve is for strong positive segregation, and the other is for negative segregation yet the enthalpies are almost equal. Therefore, the enthalpy of the primary solid is assumed to be only a function of temperature. Finally, there is only one curve for the eutectic constituent since it is assumed that the composition of the eutectic which forms at the end of solidification is unique.

The enthalpy of the alloy in the S/L temperature range ($T_E \leq T \leq T_L$) is given by the weighted average of the enthalpies of the liquid and primary solid

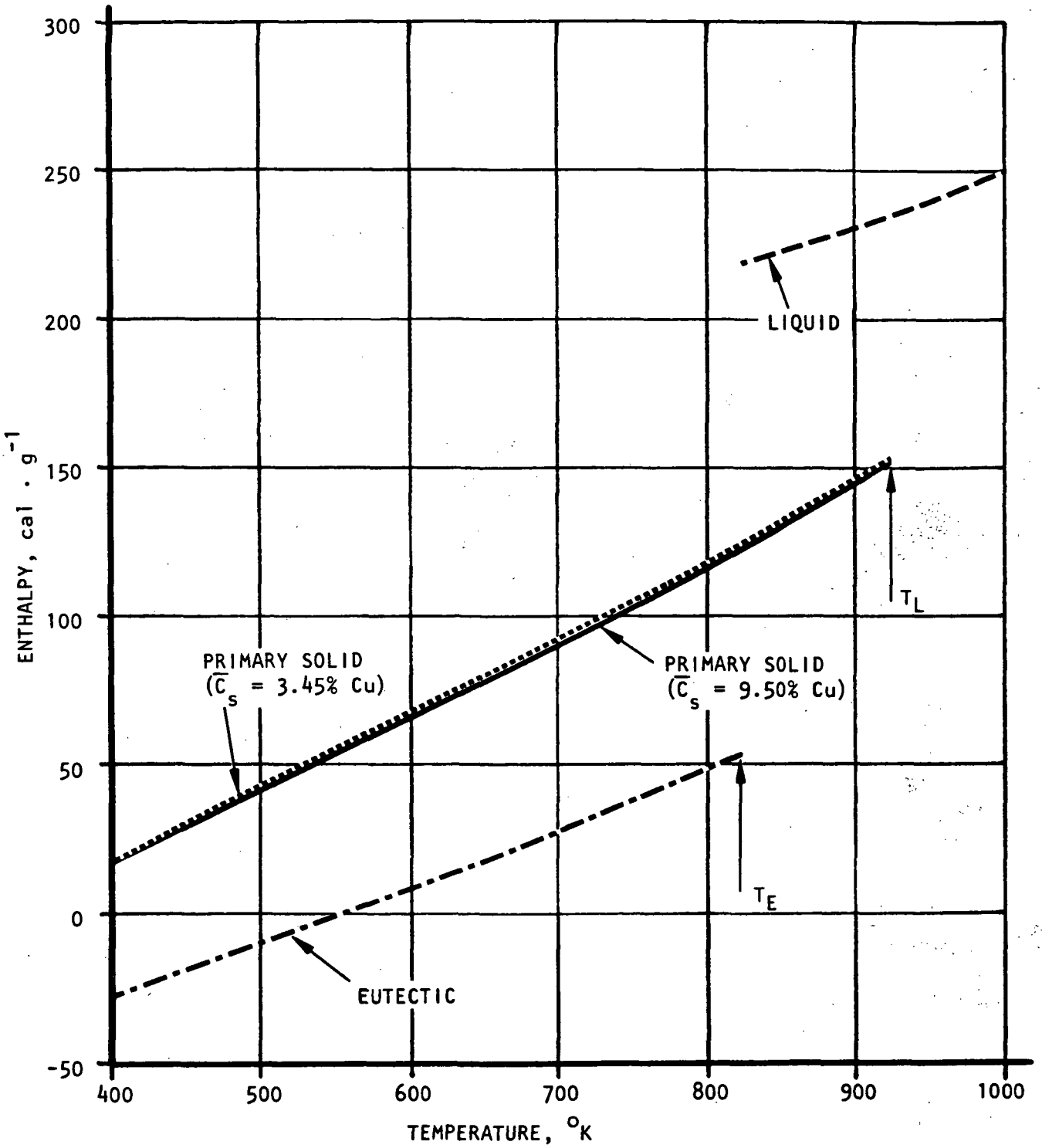

Figure B1 - Enthalpy of the liquid and solid phases and eutectic constitutent for A1-4.5% Cu

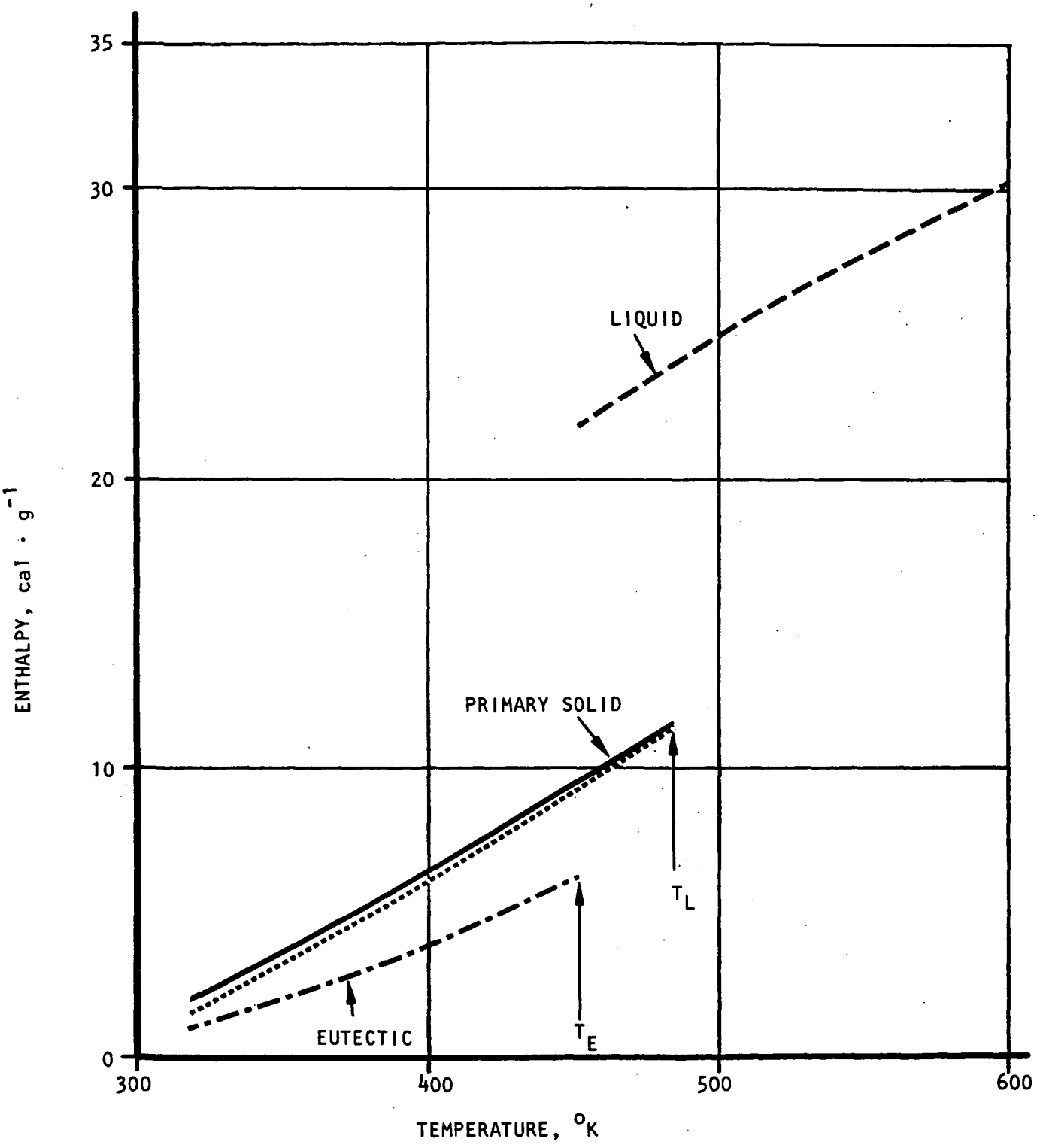

Figure B2 - Enthalpy of liquid and solid phases and eutectic constituent for Sn - 15% Pb

Solid line for the primary solid corresponds to positive segregation with $\overline{C}_s$ = 21.5% Pb and the broken line to negative segregation with $\overline{C}_s$ = 13.2% Pb.

constituents, with the relative amounts of the constituents determined by the local macrosegregation conditions. Likewise for $T \leq T_E$, the enthalpy of the alloy depends upon the relative amounts of the primary solid constituent and the eutectic constituent. Thus, the calculation of enthalpy is a dynamic calculation which is done as part of the entire macrosegregation calculation.

Figure B.2 shows the enthalpy curves for Sn-15% Pb alloy. Again the two curves for the primary solid are very close to each other so the enthalpy of the primary solid is approximated as a unique function of temperature. Calculations for Figures B.1 and B.2 were performed using the thermodynamic properties listed in Table B.1. Linear regression analyses on many coordinates along each of the curves shown in Figures B.1 and B.2 were performed to obtain the values listed in Appendix A.1.

Table B.1

Thermodynamic properties of Al-4.5% Cu and Sn-15% Pb Alloys

Alloy	Al-4.5% Cu		Sn-15% Pb		
Components	Al	Cu	Sn	Pb	Reference
a_i (cal/mol-K)	4.94	5.41	4.42	5.63	41
b_i (cal/mol-K^2)	0.00296	0.00150	0.0063	0.00233	41
c_i (cal-K/mol)	0	0	0	0	41
e_i (cal/mol-K)	7.0	7.5	8.29	7.75	41
f_i (cal/mol-K^2)	0	0	-0.0022	-0.00074	41
g_i (cal-K/mol)	0	0	0	0	41
T_{mi} (K)	933	1,356	505.1	600.6	42,44
ΔH_{fi} (cal/mol)	2,550	3,120	1,680	1,147	42,44
α_S (cal/mol)	-19,100		3,244(1)		43
α_L (cal/mol)	-5,550		1,319		43
m	2.13		--		43
n	1		--		43
ΔH_{298} (cal/mol)	-9,600		--		43
f_l	0.584		--		--
X_α	0.0248		0.985		43
X_β	--		0.71		43

(1) This is approximate since data for Pb-rich alloys are used.

GENERAL ELECTRIC